2020-09-04

Assessment of r-process sensitivity studies and metrics

Osakwe, Carlton-James U.

UNIVERSITY OF CALGARY

Assessment of *r*-process sensitivity studies and metrics

by

Carlton-James U. Osakwe

A THESIS

SUBMITTED TO THE FACULTY OF GRADUATE STUDIES

IN PARTIAL FULFILLMENT OF THE REQUIREMENTS FOR THE

DEGREE OF MASTER OF SCIENCE

GRADUATE PROGRAM IN PHYSICS AND ASTRONOMY

CALGARY, ALBERTA

SEPTEMBER, 2020

Abstract

Understanding the *r*-process is essential to understanding the early Universe. Sensitivity studies are important to developing this understanding, but they are hindered by discrepancies in how their results are reported. The fundamentals of the *r*-process and sensitivity studies are described. These discrepancies are explored in detail. We primarily discuss the way sensitivity is quantified and the normalization of results. The need for consistent results is asserted, and the issues with inconsistent results are made evident. The discrepancies themselves suggest various future avenues of study. We conclude with several recommendations for consistent reporting of sensitivity studies.

Acknowledgements

I would like to thank my supervisor, Dr. Rachid Ouyed, for all his hard work and support during my degree. His knowledgeability of the *r*-process was invaluable, and he was always available when I needed to discuss problems. I will always be grateful for his guidance.

I would also like to thank Nico Koning for his much-needed support with the various codes I used in my research.

Contents

List of Tables

List of Figures

List of Symbols, Abbreviations and Nomenclature

Symbol	Definition
A	nuclear mass number
c_s	sound speed
e^-	electron
F	sensitivity factor
FRDM	finite-range droplet (nuclear mass) model
k_B	Boltzmann's constant
HEW	high-entropy wind
HFB/HFB-21	Hartree-Fock-Bogoliubov nuclear mass model
λ	nuclear reaction rate
M_H	hydrogen mass
$M_\odot$	solar mass
μ	chemical potential
n	neutron
N	number of neutrons
n_n	neutron number density
NSE	nuclear statistical equilibrium
NSM	neutron star merger
$\bar{\nu}$	antineutrino
ODE	ordinary differential equation
$P^{\beta dn}(n=j)$	probability that j neutrons will be emitted after a β-decay
QN	quark nova
R	radius of r-process material (km)
ρ_5	density in units of 10^5 g/cm^3

S	entropy (k_B/baryon)
$\langle \sigma v \rangle$	thermally averaged neutron capture cross section
SiRop	Simulation of Rapid Neutron Capture (r-process simulation software)
SN	supernova
t	time (s)
T_9	temperature, in units of 10^9 k
UDS	up-down-strange (quark matter)
U of C	University of Calgary
v_{exp}	velocity of expansion of r-process material (km/s)
WPA	waiting point approximation
X	isotope mass fraction (for r-process nuclei)
Y	isotope abundance (for r-process nuclei)
Z	number of protons

Chapter 1

INTRODUCTION

The origin of elements is an interesting and important question, given that the elemental composition of the Universe provides a unique insight into its early evolution. The production of the elements is driven by nuclear reactions and processes. In fact, element creation in general is referred to as nucleosynthesis.

1.1 Synthesis of heavy elements

The nuclear processes responsible for creating elements heavier than iron are of particular significance because knowledge of how these elements were formed gives us insight into the astrophysical events that were common in the early Universe (by which I mean the first few hundred million years after the Big Bang [6]). While the creation of elements up to and lighter than iron is well-understood (nuclear fusion in star cores), the fusion of elements heavier than iron is not energy-efficient, and in fact, creating these heavy elements necessitates more extreme astrophysical conditions. Exactly where and to what extent different possible sites of heavy element creation occur is the subject of active research. The two main mechanisms of heavy element creation are slow neutron capture (the *s*-process) and rapid neutron capture (the *r*-process). The *s*-process is a chain of nuclear reactions in which nuclei capture neutrons whilst also decaying to more stable elements [15]. This thesis will focus on the *r*-process.

1.2 r-process nucleosynthesis

The *r*-process is a chain of nuclear reactions that is responsible for about half of the heavy element abundance in the universe [3, 4]. The primary nuclear reactions are neutron capture and beta-decay

(β^-decay in particular), that is, nuclei capture neutrons under given astrophysical conditions, and some of those neutrons decay into protons to create heavy elements. Other processes involved in the *r*-process include photodissociation and beta-delayed neutron emission, which both remove neutrons from nuclei.

The primary distinction between the *r*-process and the *s*-process is the rate of neutron capture. In the *s*-process, the rate of beta-decay is much higher than the rate of neutron capture. This is in contrast to the *r*-process, where the reverse is true. Sustaining a rate of neutron capture high enough to create elements via the *r*-process requires that the environments in which these reactions take place be both explosive and neutron-rich.

1.2.1 High-entropy wind

One such *r*-process environment is the core-collapse supernova (SN). At some point, fusion within a massive star is no longer sufficient to counteract the star's gravity, the core collapses into a proto-neutron star, while the outer layers bounce off the core and expand outwards, creating a supernova explosion. The proto-neutron star cools via neutrino emission [13], and these neutrinos heat the surrounding material. This in turn causes an adiabatically expanding stellar wind that can be a site for the *r*-process [11]. This phenomenon is relatively well studied (e.g., by Farouqi et al. (2010) [7]), and is referred to as a high-entropy wind (HEW).

1.2.2 Neutron star mergers

Another *r*-process site is the neutron star merger (NSM). Given the high concentrations of neutron-rich material in these compact objects, a collision between two or more neutron stars makes sense as a good *r*-process site. Despite the strong gravitational attraction of neutron star material, it has been theorized that about 0.01-0.001 $M_\odot$ of material could be ejected by a NSM event [8]. This would make NSMs a significant contributor to *r*-process nuclei abundances.

1.2.3 Quark novae

Quark novae (QNe) are newly theorized astrophysical events and possible sites for the *r*-process. The occurrence of these events are based on up-down-strange (UDS) quark matter, theorized to be the lowest-energy state of matter [32]. It is believed that quark matter can exist in the core of neutron stars [9]. If the core of a neutron star reaches quark deconfinement density, it undergoes a phase transition to UDS matter, resulting in a QN. The event can release up to 10^{53} ergs of energy, ejecting the neutron star's outer layers [22]. While the QN has not yet been observationally confirmed, it is believed that the QN ejecta can effectively facilitate the *r*-process [22].

1.3 Sensitivity studies and metrics

Given the high rates of neutron capture, the *r*-process ends up creating many neutron-rich nuclei far from stability (exotic nuclei). Many of these nuclei have not been experimentally measured, i.e., their properties are not exactly known. Studying the *r*-process often involves simulating the relevant reactions, and we use nuclear models to predict the properties of the nuclei we have not directly observed or measured.

Existing experimental facilities are capable of directly measuring exotic nuclei, but these measurements are resource-intensive. Identifying specific nuclei whose properties need to be known exactly is therefore of great importance. Sensitivity studies are the mechanism by which we determine which nuclei should be prioritized for measurement. They employ *r*-process simulations to deduce which nuclei have the greatest effect on the simulation results.

Each *r*-process simulation creates what is called an abundance pattern. This is a graph displaying the proportion of matter for each nuclear mass number A. This could be either the number proportion, known as the abundance Y, or the mass proportion, known as the mass fraction $X = AY$. Sensitivity studies look at the differences in abundance patterns to quantify the importance of specific nuclei to the *r*-process.

The basic process of a sensitivity study is as follows: an *r*-process simulation is run, and its

resultant abundance pattern is used as a control (this is often referred to as a baseline). Then an input parameter (e.g., mass) is changed for a specific isotope, and the simulation is run again. The "sensitivity" of the isotope is proportional to the difference between the control abundance pattern and the abundance pattern of the simulation in which the input parameter was changed, i.e., the greater the difference, the more "sensitive" the *r*-process is to that specific isotope when that specific input parameter is changed.

Quantifying sensitivity requires quantifying the difference between *r*-process abundance patterns. To do this we use what are called sensitivity metrics. These metrics boil down the abundance pattern differences to a number (i.e. a sensitivity factor, denoted by F) that can be compared to those of other isotopes. In my research I looked at four different sensitivity metrics:

$$\begin{aligned} F^{A1} &= \sum_{N,Z} |X - X_{\text{base}}| \\ F^{A2} &= \sum_{N,Z} |Y - Y_{\text{base}}| \\ F^{R1} &= \sum_{N,Z} \left| \frac{Y - Y_{\text{base}}}{Y_{\text{base}}} \right| \\ F^{R2} &= \sum_{N,Z} \left| \log_{10} \frac{Y}{Y_{\text{base}}} \right| \end{aligned} \tag{1.1}$$

The sums are over a range of isotopes with neutron number N and proton number Z. X_{base} and Y_{base} refer to the mass fraction and abundance of the baseline result (for each isotope in the range), respectively. The first three of these metrics have been used in other sensitivity studies.

This thesis will look primarily at sensitivity studies and how their results are reported. Section 2 outlines the physical and astrophysical conditions and principles underpinning the *r*-process and sensitivity studies. In Section 3.1 I make an effort to reproduce the results of existing studies. Section 4 is an in-depth look at the issue of standardization of sensitivity study results. Section 5 explores another issue (namely the normalization of sensitivity study results) that is touched on in Section 4. These are followed by my conclusions and possibilities for future work.

Chapter 2

MODELING THE R-PROCESS

2.1 The nuclear physics

SiRop is a publicly available *r*-process simulation code developed by the Quark Nova group at the University of Calgary [27]. I used this software to run sensitivity studies for this thesis.

Modeling the *r*-process involves solving a large number of coupled ordinary differential equations (ODEs). The rate of change of the abundance of any one isotope in the *r*-process chain is in the most general sense given by Equation 2.1, where $\dot{Y}(Z,A)$ is a time derivative,

$$\dot{Y}(Z,A) = \text{processes that create } Y(Z,A) - \text{processes that destroy } Y(Z,A). \tag{2.1}$$

All of the nuclear reactions that feature most prominently in the *r*-process are neutron capture, beta decay, photodissociation and beta-delayed neutron emission[1] serve to both increase and decrease the amount of any given isotope.

Neutron capture is the phenomenon where nuclei capture neutrons, increasing their mass number as shown in Equation 2.2,

$$^{A}_{Z}X + n \rightarrow {}^{A+1}_{Z}X. \tag{2.2}$$

In this subsection X refers to a given isotope with Z protons and an atomic mass of A. Hereafter X will refer to mass fraction.

β^--decay is the main form of beta-decay in the *r*-process, and this involves neutrons converting to protons by ejecting an electron and an antineutrino (Equation 2.3),

$$^{A}_{Z}X \rightarrow {}^{A}_{Z+1}X' + e^- + \bar{\nu}. \tag{2.3}$$

[1] I should note that alpha-decays also occur in the *r*-process, though not as often as the other reactions.

Hereafter the terms "beta-decay" and "β-decay" will refer to β^--decay. As mentioned before, these two reactions are the primary mechanisms of the *r*-process. In addition to these, we have photodissociation, a process in which a neutron is removed from a nucleus by a gamma photon (Equation 2.4),

$$ {}^{A}_{Z}X + \gamma \rightarrow {}^{A-1}_{Z}X + n. \tag{2.4} $$

Beta-delayed neutron emission occurs when an initial nucleus beta-decays to an excited state of its beta-decay product nucleus. If this excited state has enough energy, one or more neutrons can be emitted when the product nucleus decays to its ground state. This is shown in Equation 2.5,

$$ {}^{A}_{Z}X \rightarrow {}^{A}_{Z+1}X'^{*} + e^- + \bar{\nu} \rightarrow {}^{A-j}_{Z+1}X' + jn, \tag{2.5} $$

where j neutrons are emitted, and the '*' indicates that the nucleus is in an excited state. Alpha-decay occurs when a nucleus ejects and alpha particle (Equation 2.6),

$$ {}^{A}_{Z}X \rightarrow {}^{A-4}_{Z-2}X' + {}^{4}_{2}\alpha. \tag{2.6} $$

Finally, nuclei that are particularly big $A > 200$ tend to fission into smaller nuclei that then proceed along the *r*-process themselves.

Given these reactions, the rate of change of a given isotope could be described as shown in Equation 2.7,

$$ \begin{aligned} \dot{Y}(Z,A) = {} & n_n \langle \sigma v \rangle Y(Z,A-1) + \lambda^{\gamma}_{Z,A+1} Y(Z,A+1) + \lambda^{\alpha}_{Z+2,A+4} Y(Z+2,A+4) \\ & + \sum_{j=0}^{3} P^{\beta dn}_{Z-1,A+j} (n=j) \lambda^{\beta}_{Z-1,A+j} Y(Z-1,A+j) - n_n \langle \sigma v \rangle Y(Z,A) - \lambda^{\gamma}_{Z,A} Y(Z,A) \\ & - \lambda^{\alpha}_{Z,A} Y(Z,A) - \sum_{j=0}^{3} P^{\beta dn}_{Z,A} (n=j) \lambda^{\beta}_{Z,A} Y(Z,A) + \text{fission}. \end{aligned} \tag{2.7} $$

Here n_n is the neutron number density, $\langle \sigma v \rangle$ is the thermally averaged neutron capture cross section

(referring to the cross-section around a target nucleus inside which neutron capture is likely to occur multiplied by the velocity of the incident neutrons), λ^{γ} is the photodissociation rate, λ^{α} is the α-decay rate, λ^{β} is the β-decay rate, and $P^{\beta dn}_{Z-1,A+j}(n=j)$ is the probability that j neutrons will be emitted following a β-decay (beta-delayed neutron emission). The fission terms represent any nuclei of the isotope created when larger unstable nuclei fission into smaller nuclei, as well as those that are destroyed when the isotope itself undergoes fission.

Calculating the evolution of an *r*-process network involves solving this equation for every isotope in the network simultaneously. This necessitates solving a matrix of over 64 million elements each time step (many of these elements will be zero, but this is still computationally intensive). SiRop solves this network using a form of Gaussian elimination and sparse matrix algorithms (this code is based on another *r*-process code called r-Java, where it was determined that this method was fastest [11]).

SiRop also allows the user to take advantage of an approximation that also simplifies computations known as the waiting point approximation (WPA). Empirically, the WPA assumes that the *r*-process chain (or path) consists of solely neutron capture until the path reaches what are called "waiting points". These waiting points refer to nuclei where rates of neutron capture and loss via beta-decay are equal. It should be noted that these waiting points may be reached before the magic numbers[2] if the temperature is high enough for the rate of neutron capture to be matched by the rate of photodissociation. The WPA then assumes that there will be no net loss of neutrons until the path reaches a nucleus with a lower beta-decay rate. The "waiting points" are traditionally doubly magic nuclei [5]. Figure 2.1 provides a visual representation.

This approximation requires that the environment in which the *r*-process takes place be extremely neutron-rich ($n_n > 1 \times 10^{20}$ cm^{-3}, so that neutron captures can continue all the way to the waiting points) and be high-temperature ($T > 2 \times 10^9$ K, so that the rates of photodissociation are sufficiently high).

[2]Nucleons are believed to have a shell structure similar to that of electrons; the magic numbers refer to the number of protons or neutrons at which a proton or neutron shell is closed, respectively. Nuclei with a closed proton or a closed neutron shell are referred to as magic nuclei, those with both closed proton and neutron shells are doubly magic.

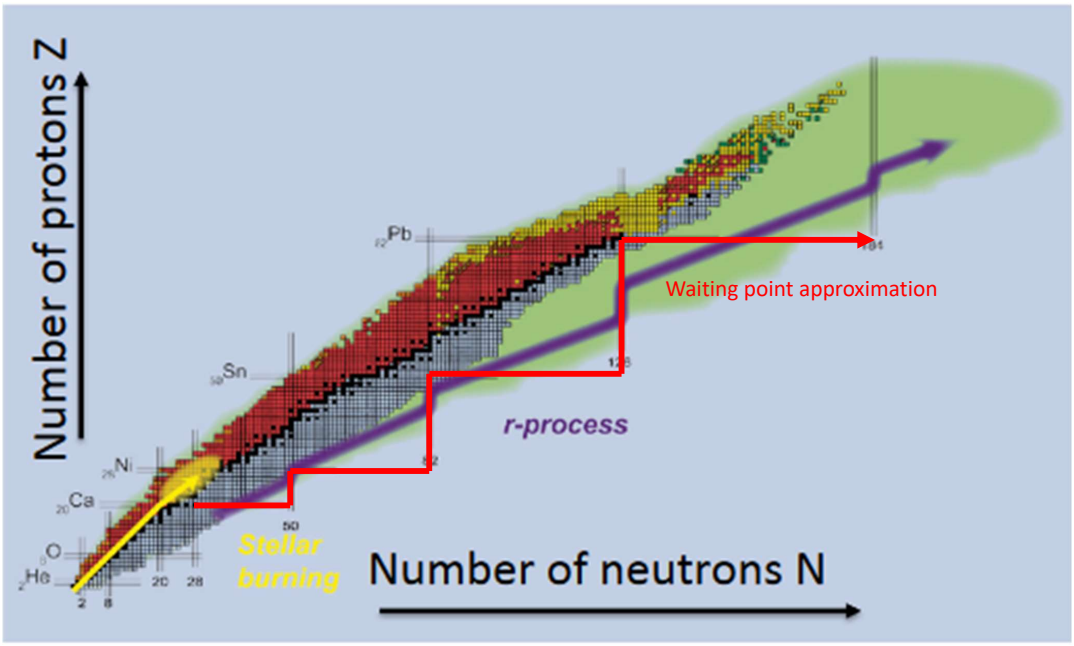

Figure 2.1: Visual representation of the waiting point approximation (red) compared to the actual *r*-process path (purple). The figure was modified from the Institut für Kernphysik, Technische Universität Darmstadt website.

2.1.1 Nuclear mass models

It was mentioned that we use nuclear models to predict the properties of nuclei we have not measured or observed. With regards these nuclear mass models in particular, examples include the finite-range droplet model (FRDM), as well as the Hartree-Fock-Bogoliubov (HFB) mass models. The FRDM is a mass model that allows for nuclear compression (it is understood that nuclei can undergo deformation, and are not always spherical) and takes into account the finite range of the nuclear force. This model is commonly referred to as a macroscopic-microscopic model, since it predicts nuclear properties with both macroscopic (looking at a whole nucleus) and microscopic (looking at interactions between nucleons) models [18]. The HFB-21 mass model is one of a series of mass models that attempts to predict the properties of exotic nuclei using only basic nucleon-nucleon interactions, and is therefore referred to as a microscopic model [25]. In this study I refer to the HFB-21 mass model, as this is the one used by the SiRop code.

Their mathematical formulations are not relevant to this thesis. However, the mass models are still important because, while they generally all predict the properties of known nuclei, there are divergences in their extrapolations to those that have not been measured, particularly neutron-rich nuclei. As such, they influence the way sensitivity studies are conducted, i.e., the extent to which input parameters are changed will often reflect differences between the predictions of the models.

2.2 The astrophysics

There are a number of astrophysical factors that influence whether and to what extent a site can facilitate the *r*-process. One of the most significant factors is the initial composition of the environment. This is described by the neutron-to-seed ratio ($Y_{\mathrm{n}}/Y_{\mathrm{seed}}$) defined by Equation 2.8,

$$\frac{Y_{\mathrm{n}}}{Y_{\mathrm{seed}}} = \frac{Y_{\mathrm{n}}(t_0)}{\sum_{Z,A} Y(Z,A)} = \frac{1-X_0}{X_0/A}, \tag{2.8}$$

where X_0 is the initial mass fraction of the seed (the initial composition of material other than neutrons is referred to as the "seed") [11] and t_0 is the initial time. This is the ratio between neutrons and other nuclei in an *r*-process environment. Since neutron capture is the main mechanism of the *r*-process, the amount of neutrons in the system relative to the seed nuclei determines how far the *r*-process can proceed; a higher neutron-to-seed ratio allows for a more robust *r*-process and creates heavier elements. The *r*-process uses up neutrons as it occurs, and will stop if there are no longer enough neutrons to continue.

The specific type of seed nuclei also determines the robustness of the *r*-process. In general, the heavier the seed nuclei (i.e., the larger the mass number of the seed), the heavier the elements created when neutrons are added to those nuclei (given a sufficiently large neutron-to-seed ratio). As well, the *r*-process needs to be simulated for a long enough time to run to completion (SiRop allows for a time cutoff in addition to other stopping conditions, the main *r*-process can run to completion in about 10 s in-simulation).

Temperature and density also influence whether or not the *r*-process can take place. The *r*-process tends to take place at high temperatures (these are often measured in units of 10^9 K), but the temperature can still be too high; at a certain point nuclear statistical equilibrium (NSE) sets in. In NSE all nuclear processes and their inverses are in equilibrium with each other, and the *r*-process can not proceed in any particular direction. This is mathematically described by the equation of detailed balance (Equation 2.9) which holds in NSE,

$$Z_i\mu_p + N_i\mu_n = \mu_i. \tag{2.9}$$

Here μ_i represents the chemical potential of isotope i.

2.2.1 Temperature and density

SiRop offers some flexibility with regards to initial conditions, including temperature and density evolution (though these are generally related). That said, different *r*-process sites will have their

own initial conditions, whether the site is a HEW, a NSM, or a QN. In this thesis I mainly looked at the HEW scenario, as well as a more generalized *r*-process environment that SiRop offers.

In SiRop's default *r*-process environment (referred to as the "custom" environment), it is assumed that the *r*-process material expands adiabatically (simulating the adiabatic expansion of a hot bubble of material), with the entropy remaining constant. The density $\rho(t)$ is based on that from Meyer et al. (1997) [17], who derived the density evolution shown in Equation 2.10 assuming an adiabatic expansion with constant entropy,

$$\rho(t) = \frac{\rho_0}{(1+t/(2\tau))^2}, \tag{2.10}$$

and is related to the temperature by Equation 2.11,

$$\rho \propto T^3, \tag{2.11}$$

where ρ_0 is the initial density, t is the time, τ is the expansion timescale, and T is the temperature. This density evolution was later generalized by Kostka [11] to Equation 2.12,

$$\rho(t) = \frac{\rho_0}{(1+(at/\tau)^b)^c}. \tag{2.12}$$

Here a, b, and c are free parameters.

For the HEW scenario, the temperature evolution in SiRop is consistent with Farouqi et al. (2010) [7]. It assumes the temperature evolves adiabatically, and is governed by Equation 2.13,

$$T_9(t) = T_9(t=0)\frac{R_0}{R_0 + v_{\exp}\, t}, \tag{2.13}$$

where T_9 is the temperature in units of 10^9 K, R_0 is the initial radius of the material in km, $v_{\exp}$ is the expansion velocity of the material in km/s, and t is time in s.

The density, also consistent with Farouqi et al. (2010) [7], is calculated assuming that the

entropy of the material is radiation-dominated; that is, at sufficiently high temperatures the pressure from relativistic particles is higher than the pressure from non-relativistic particles. The density ρ_5 evolves as in Equation 2.14,

$$\rho_5(t) = 1.21 \frac{T_9^3}{S} \left(1 + \frac{7}{4} \frac{T_9^2}{T_9^2 + 5.3}\right). \tag{2.14}$$

Here ρ_5 is in units of 10^5 g/cm^3 and S is the entropy in units of Boltzmann's constant per baryon. It should be noted that there are other ways to evolve the temperature and density depending on the specific *r*-process environment, we will explore these in Section 3.1.

Chapter 3

BENCHMARKING THE CODE

3.1 Rationale

I had set out to reproduce the results of an earlier submitted paper [27]. While doing so I encountered an inconsistency between some of the sensitivity factors as determined by the original author and those calculated during my revisions. I therefore had to figure out why this was the case.

This motivated an effort to recreate the results of other sensitivity studies in an effort to benchmark the SiRop code. I was unable to do so in the end, but I believe this is due to insufficient descriptions of initial conditions, as well as temperature and density evolution.

3.2 Benchmarking the paper (Paper I)

One discrepancy in the simulations is related to the expansion timescale τ. This parameter governs the rate of expansion of the material in which the *r*-process takes place, e.g., the matter expanding from a supernova site, a neutron star merger, or a quark nova. In the paper it was recorded as 0.001 s, but our tests, which included reproducing sensitivity factors and recreating figures in the paper, found that using a τ of 0.01 s yielded results more consistent with the original numbers, and therefore concluded that the $\tau = 0.001$ s was a typo. The distinction between the two versions of τ is shown in Table 3.1, and the τ recorded in the paper is now equal to 0.01 s.

Normalization and calibration of the sensitivity factor F were also major components of our effort to recreate the original sensitivity factors. Section IV of Shand et al. (2017) [27] proposes a standard way to normalize computed sensitivity factors using arbitrary scaling constants a and b[1]. These constants are defined in Equation 3.1 for the four metrics menitoned previously:

[1]Note: these are newly defined arbitrary constants, and are distinct from the free parameters a, b, and c from Equation 2.12 in Section 2.

τ	A1	A2	R1	R2
0.01	44.7	0.331	17.5	7.29
0.001	2.68E-6	2.03E-8	4.73E-7	2.06E-7

Table 3.1: Sensitivity factors obtained (without normalization) from changing the mass of Sn-132 by $+0.0005\%$. The top row has an expansion timescale $\tau = 0.01$ s, and the bottom has $\tau = 0.001$ s.

$$
\begin{aligned}
F^{A1} &= \sum_{N,Z} |aX - bX_{\text{base}}| = \sum_{N,Z} b \left| \frac{a}{b} X - X_{\text{base}} \right| \\
F^{A2} &= \sum_{N,Z} |aY - bY_{\text{base}}| = \sum_{N,Z} b \left| \frac{a}{b} Y - Y_{\text{base}} \right| \\
F^{R1} &= \sum_{N,Z} \left| \frac{aY - bY_{\text{base}}}{bY_{\text{base}}} \right| = \sum_{N,Z} \left| \frac{\frac{a}{b} Y - Y_{\text{base}}}{Y_{\text{base}}} \right| \\
F^{R2} &= \sum_{N,Z} \left| \log_{10} \frac{aY}{bY_{\text{base}}} \right| = \sum_{N,Z} \left| \log_{10} \frac{a}{b} Y - \log_{10} Y_{\text{base}} \right|
\end{aligned}
\tag{3.1}
$$

In the end, the paper recommends that a and b (or more specifically, a normalization factor a/b) be chosen so as to minimize the sensitivity factor F. Our other tests (different codes, different initial parameters) were performed both with and without normalization. In the end, we added a function to automatically find the a/b value that minimizes F.

Shand et al. (2017) [27] also recommends that the maximum abundance in r-process simulations be recorded along with the sensitivity study results to further ease comparison (this is referred to as calibration). We had to resolve a difference between our calculated maximum abundance and the one stated in the paper. Our value was eventually selected, as it was more consistent with the relevant reference in the aforementioned section.

To verify the consistency of the results from the different r-process simulation codes available to me, I also compared the SiRop code to the r-Java code described in Kostka et al. (2014) [12].

	A1	A2	R1	R2
Old version	38.0	0.280	89.4	37.0
New version	37.9	0.283	17.5	7.31
Original numbers	26.7	0.194	14.9	6.61

Table 3.2: Sensitivity factors obtained from changing the mass of Sn-132 by $+0.0005\%$. The top row is from an older version of the SiRop *r*-process code, the middle is from latest version of that code, and the bottom are the original numbers.

3.3 Code changes

It should be mentioned that SiRop had undergone some code changes since the original sensitivity factors were determined. Part of the recreation of the original factors involved recovering earlier versions of the software and varying the input parameters of both codes to see if there were significant discrepancies.

One notable difference between the old and new versions of the code is the specific way the sensitivity factors are determined. This had changed from $F = \sum_{N,Z} F(Y, Y_{\text{base}})$ to $F = F\left(\sum_{N,Z} Y, \sum_{N,Z} Y_{\text{base}}\right)$. This changes the order in which the sensitivity factor is calculated. In the original code, the metric was applied to abundance differences (between the baseline and modified simulation) for individual isotopes, and these differences were added up across the range of isotopes studied. The new version adds up the abundances of all isotopes studied and applies the metric to the sums from the two simulations. This was likely an effort to optimize the code, as the latter method is computationally simpler. We determined that the new version is more consistent with the results, which are shown in Table 3.2, and we used the latest version going forward.

There were also concerted efforts to optimize the SiRop code. In particular, running full-network simulations (as opposed to the waiting point approximation) took a long time (typically weeks). We were able to speed up the code significantly (about $77\times$ faster)[2].

[2]This was done primarily by having different *r*-process simulations (e.g. the baseline simulation and any modified simulations) running in parallel instead of one after the other.

3.4 Initial conditions

We also sought to recover the results of a number of other sensitivity studies for verification [1, 12, 23]. This effort was complicated by the need to precisely identify the initial conditions of each study, which turned out to be easier said than done. What follows is a series of attempts that showcase the issues determining the initial conditions of *r*-process sensitivity studies.

I coded a different temperature evolution function into SiRop, in particular the exponential evolution used by Panov et al. (2009) [23] (shown in Equation 3.2),

$$T_9(t) = (T_9)_0 \exp(-t/\tau), \tag{3.2}$$

where τ is the expansion timescale and T_9 is the temperature in units of 10^9 K. This was in turn modified to have the temperature remain constant after a certain point, this being consistent with Panov et al. (2009) as well [23]. This is then used in SiRop to determine the density, using the formulation in Kostka at al. [12] (shown in Equation 3.3),

$$\rho_5(t) = 1.21 \frac{T_9^3}{S} \left(1 + \frac{7}{4} \frac{T_9^2}{T_9^2 + 5.3}\right), \tag{3.3}$$

where S is the entropy and ρ_5 is in units of 10^5 g cm^{-3}.

I also looked at the full temperature and density evolution of a HEW environment from Panov et al. (2009) [23]:

$$\rho(t) = \rho_{\text{ini}} \exp(-3t/\tau_{\text{dyn}}), \tag{3.4}$$

$$T_9(t) = T_9^{\text{ini}} \exp(-t/\tau_{\text{dyn}}). \tag{3.5}$$

Note: in Panov et al. (2009) [23], T_{ini} is the initial temperature (and is denoted by $(T_9)_0$ in Equation 3.2), while T_0 is the asymptotic temperature (the constant temperature the system eventually reaches). τ is the expansion timescale, referred to in the reference as the dynamical timescale. As well, for a HEW *r*-process environment, the velocity evolution (of the HEW) from Panov et al.

(2009) is given as [23]:

$$v(t) = v_{\rm ini} \exp\left(-t/\tau_{\rm dyn}\right). \tag{3.6}$$

Certain studies refer to a parameter α [10], which is related to the expansion timescale τ by the relation in Equation 3.7,

$$\tau \approx \frac{0.016 \text{ ms}}{\alpha^{1/2}}. \tag{3.7}$$

The full derivation is below (From Jaikumar et al. (2007) [10]). Here R is the radius of the r-process material in km, c_s is the sound speed, k_B is Bolztmann's constant, and M_H is the hydrogen mass. We assume that a given chunk of rapidly expanding matter (i.e., r-process ejecta expanding under pressure) has uniform density, so that

$$\rho = \rho_0 \left(\frac{R_0}{R}\right)^3. \tag{3.8}$$

Applying the momentum equation (for an expanding spherical chunk without external gravity) gives

$$\frac{d^2R}{dt^2} = \frac{\alpha c_s^2}{R}, \tag{3.9}$$

$$(dR)^2 = \alpha c_s^2 (dt)^2, \tag{3.10}$$

$$dR = \alpha^{1/2} c_s \, dt, \tag{3.11}$$

$$R = R_0 + \alpha^{1/2} c_s \, t, \tag{3.12}$$

where c_s is given by

$$c_s = \sqrt{\frac{k_B T}{A M_H}} = 3.84 \times 10^7 \sqrt{\frac{T}{10^9 \text{ K}}} \sqrt{\frac{56}{A}}, \text{ where } T = 10^9 \text{ and } A = 56. \tag{3.13}$$

Substituting Equation 3.12 into Equation 3.8,

$$\begin{aligned}\rho &= \rho_0 \left(\frac{R_0}{R_0 + \alpha^{1/2} c_s t} \right)^3 \\ &= \rho_0 \left(\frac{1}{1 + \alpha^{1/2} \frac{c_s}{R_0} t} \right)^3 .\end{aligned} \tag{3.14}$$

This implies that τ is given by

$$\begin{aligned}\tau &= \frac{R_0}{c_s \alpha^{1/2}}, \\ &= \frac{(10^3 \text{ cm}) \left(\frac{R_0}{10^3 \text{ cm}} \right) \sqrt{\frac{A}{56}}}{3.84 \times 10^7 \sqrt{\frac{T}{10^9 \text{ K}}} \alpha^{1/2}}.\end{aligned} \tag{3.15}$$

We thus recover Equation 3.7,

$$\tau \approx \frac{0.016 \text{ ms}}{\alpha^{1/2}}. \tag{3.7}$$

The results of these comparisons are shown in Figures 3.1 and 3.2. In Figure 3.1, the initial nuclear composition (initial seed) is 50% ^{70}Fe. In Figure 3.2, the initial seed is a equal distribution of isotopes of $Z \approx 34$ and $A \approx 90$. Specifically this entails isotopes with Z ranging from 32-36 (Ge, As, Se, Br, Kr), each with A ranging between 88 and 92.

The closest results to Aprahamian et al. (2014) [1] resulted from using the initial parameters from the paper I was working on [27], shown in Figure 3.3 (the initial parameters as compared to Aprahamian et al. (2014) [1] are given in Tables 3.3-3.6). It should be noted that the abundance pattern created using our initial parameters was in the WPA regime; this could have inadvertently been the case for Aprahamian et al. (2014) [1]. As well, it should be noted that Aprahamian et al. (2014) used the FRDM nuclear mass model, while SiRop uses the HFB-21 mass model.

Parameters	Environment	ρ_0 (g cm^{-3})
Aprahamian et al. (2014)	HEW	340
SiRop	Custom	1×10^{11}

Table 3.3: Table of parameters for recreating Aprahamian et al. (2014) [1].

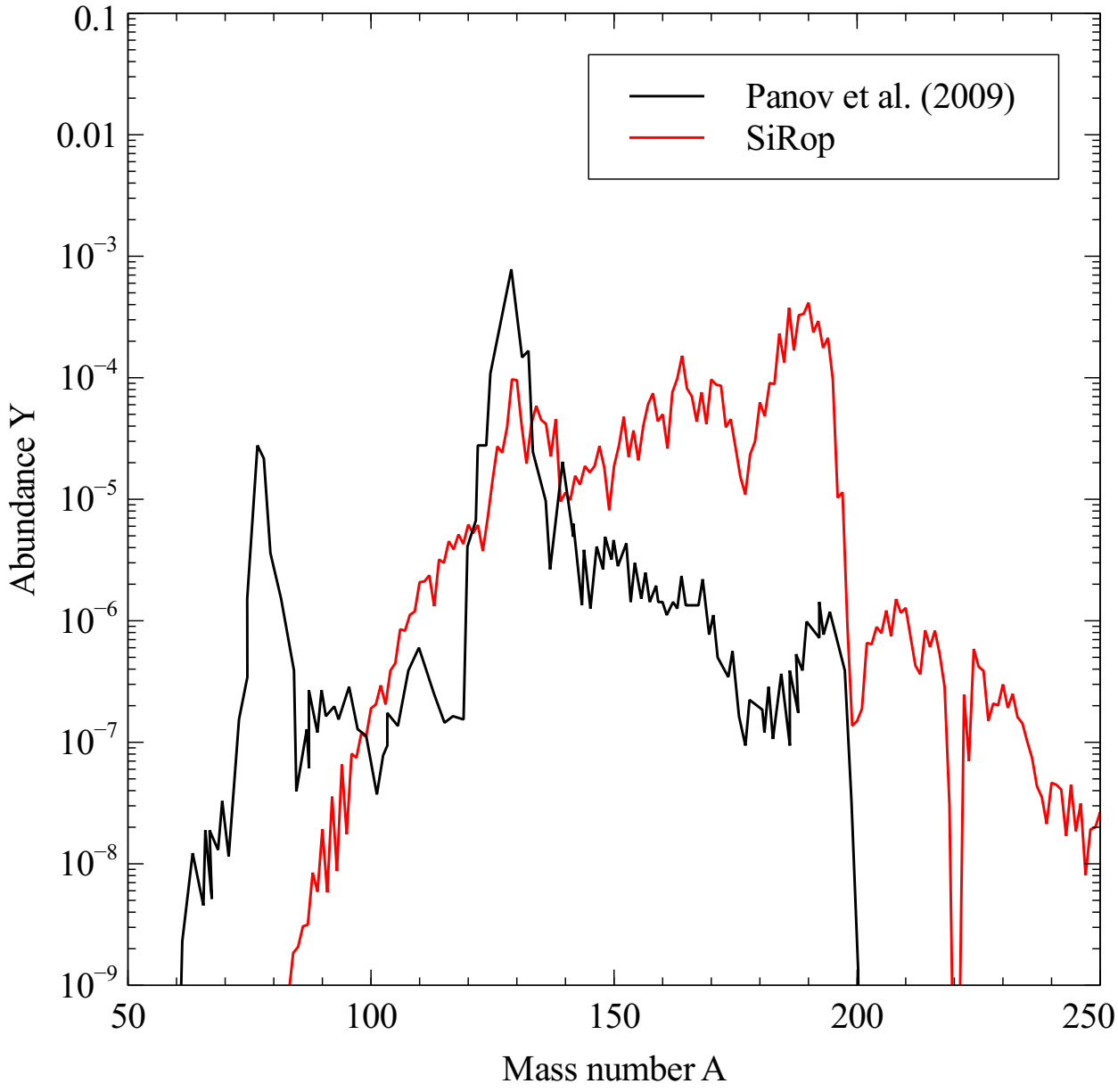

Figure 3.1: Comparison of *r*-process simulation results between those generated in SiRop and those from Panov et al. (2009) [23]. The simulations were run in a HEW *r*-process environment with initial temperature $T_9^0 = 3$, initial density $\rho_0 = 1 \times 10^{11}$ g cm^{-3}, initial electron fraction $Y_e = 0.42$, and an expansion timescale $\tau = 0.01$ s.

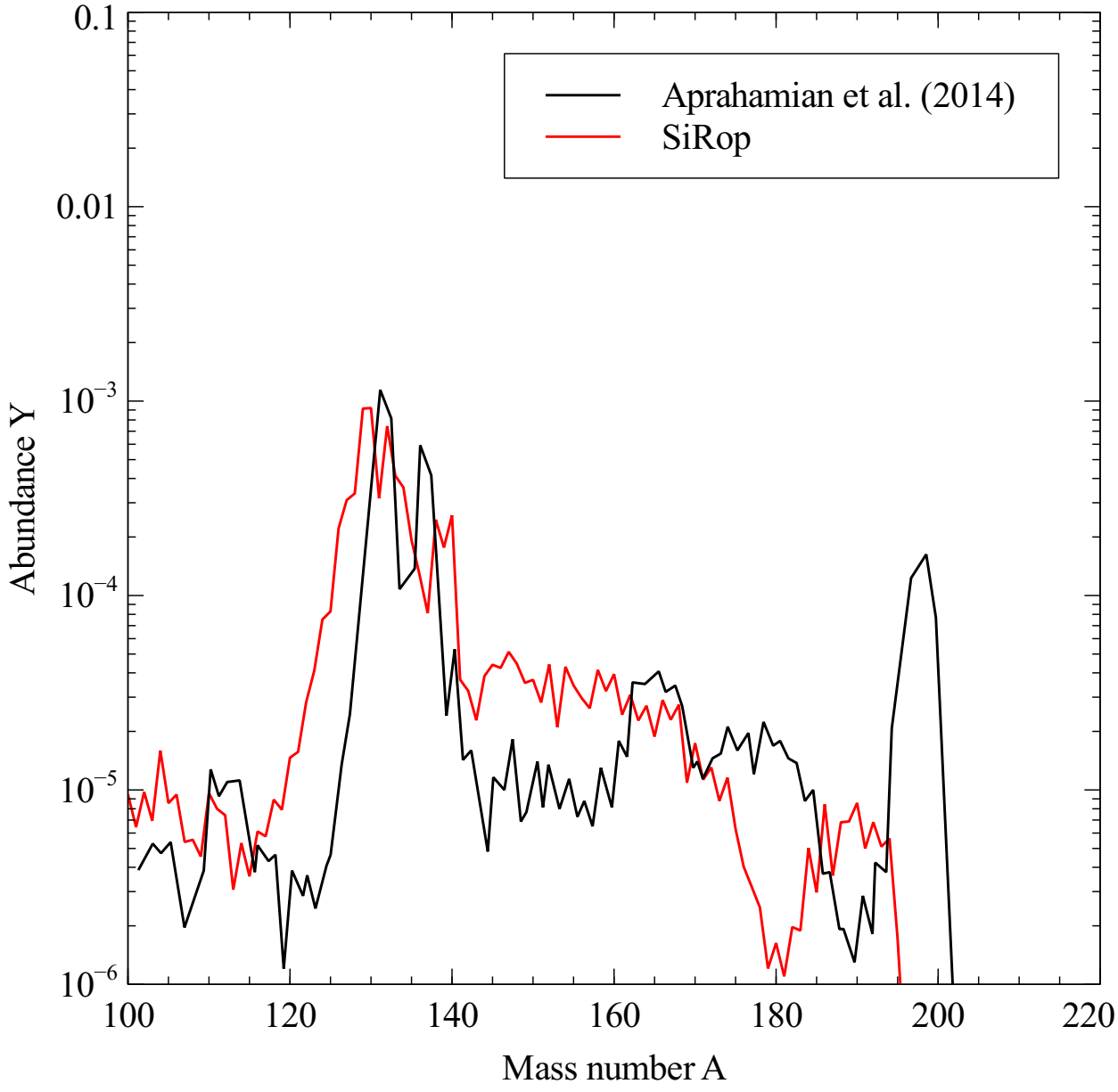

Figure 3.2: Comparison of *r*-process simulation results between those generated in SiRop and those from Aprahamian et al. (2014) [1]. The simulations were run in a HEW *r*-process environment with initial temperature $T_9^0 = 6$, initial velocity of 2000 km/s, initial radius $R_0 = 10$ km, initial entropy of 105 k_B/baryon, initial electron fraction $Y_e = 0.42$, and an expansion timescale $\tau = 0.005$ s.

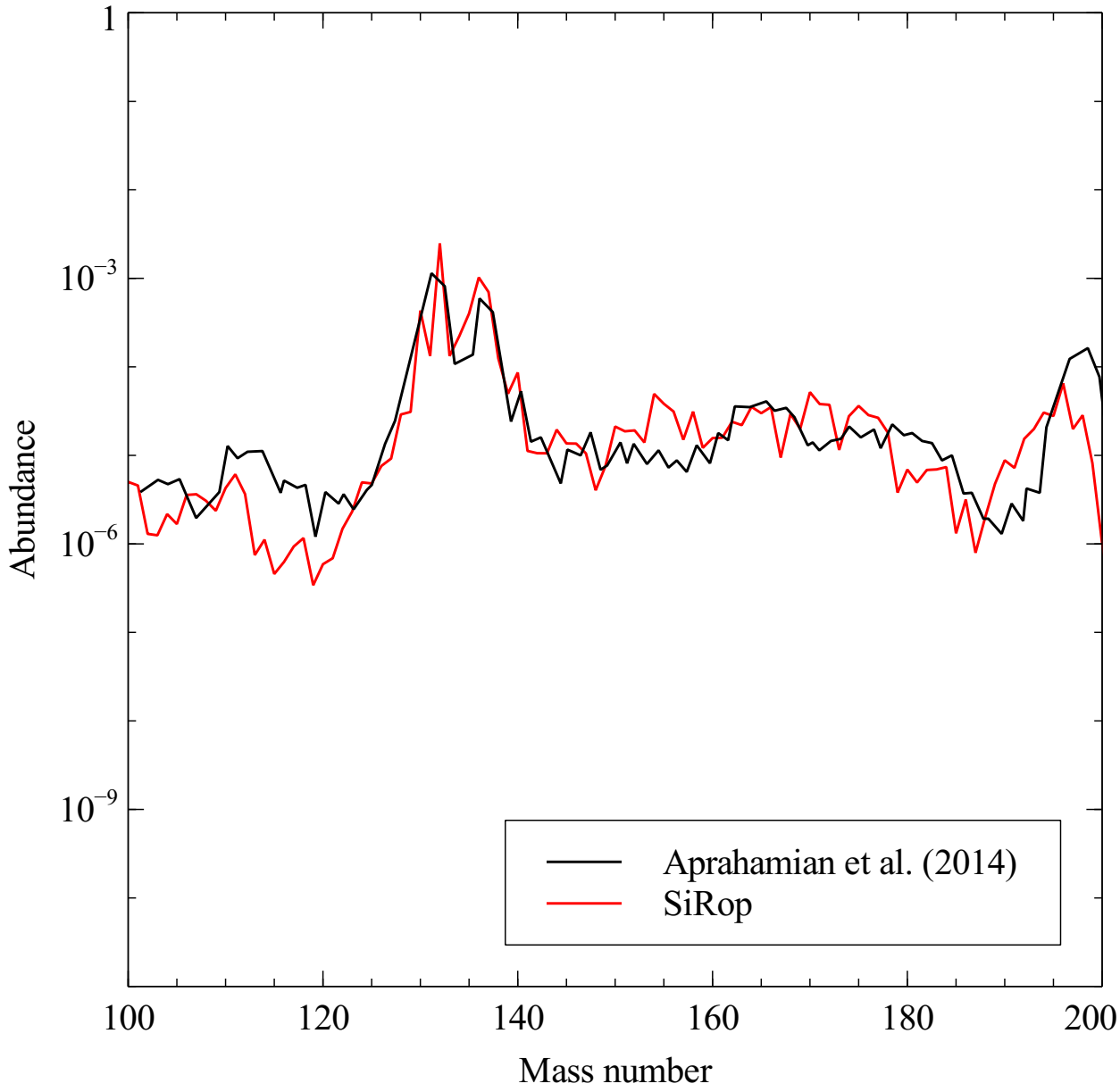

Figure 3.3: Comparison of *r*-process simulation results between those generated in SiRop and those from Aprahamian et al. (2014) [1]. The sets of initial parameters are shown in Tables 3.3-3.6.

Parameters	τ (s)	T_0 (K)	Y_e
Aprahamian et al. (2014)	0.86	1.5×10^9	0.19
SiRop	0.01	3×10^9	0.3

Table 3.4: Table of parameters (continued).

Parameters	seed	duration (s)	t_{decay} (s)
Aprahamian et al. (2014)	51% ^{70}Fe	1000	1000
SiRop	50% ^{70}Fe	10	10

Table 3.5: Table of parameters (continued).

While recreating these results I was constantly varying initial parameters to get a desirable neutron-to-seed ratio; I generally used a single isotope as the seed. At the same time, we considered whether or not the authors in the other studies had initial isotopic compositions generated from other simulations of nuclear processes, including whether or not the initial composition was created from simulating NSE. This also includes the α-process, where helium nuclei are used to create heavier elements (a range from $A = 70$ to $A = 100$). Adding an α-process code to SiRop would be a useful future project.

We later determined that Panov et al. (2009) et al. (2009) [23] assumed that the α-process started at an initial temperature of 6×10^9 K ($T_9 = 6$), while the *r*-process started at a temperature of around 2×10^9 K ($T_9 \approx 2$). I then ran more simulations with this new *r*-process temperature, using different initial seeds, including just protons and neutrons (shown in Figures 3.4 and 3.5). As well, the simulations were run with and without first running NSE, where the initial temperature $T_9^0 = 6$, the initial density was 10^6 g cm^{-3} (Later I tried 10^{12} g cm^{-3} because the neutron-to-seed ratio became too low at the onset of the *r*-process), and the initial electron fraction was 0.42. In most of the simulations where NSE was run first the *r*-process doesn't seem to progress very far, as seen in Figure 3.5.

We also sought to recreate the results of Meyer 2002 [16]. To this end I implemented the density evolution in Equation 3.16,

$$\rho(t) = \rho_1 \exp(-t/\tau) + \rho_2 \left(\frac{\Delta}{\Delta + t}\right)^2, \tag{3.16}$$

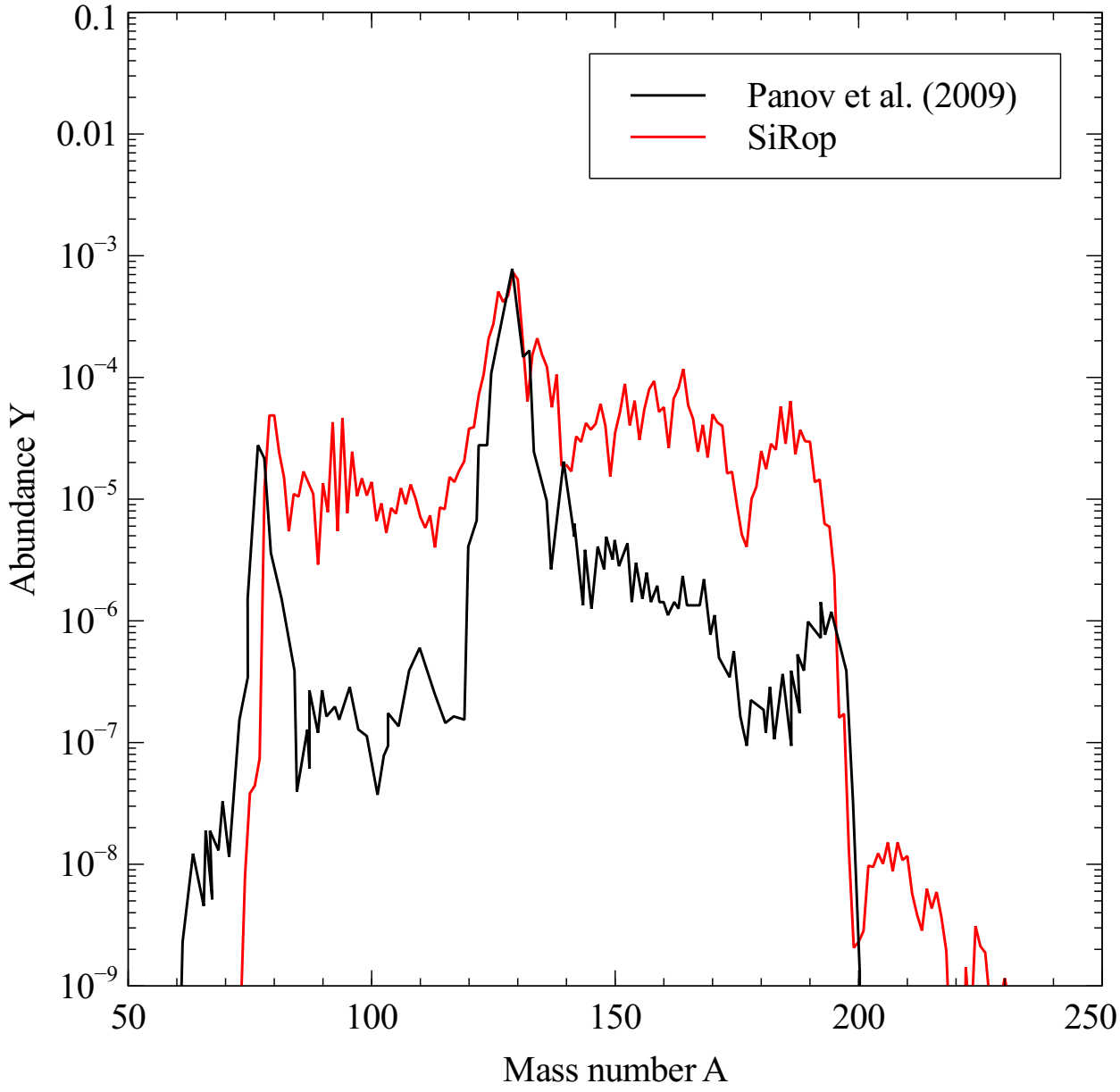

Figure 3.4: Comparison of *r*-process simulation results between those generated in SiRop and those from Panov et al. (2009) [23]. The simulations were run in a HEW *r*-process environment with initial temperature $T_9^0 = 2$, initial electron fraction $Y_e = 0.42$, and an expansion timescale $\tau = 0.005$ s. As well, the initial entropy $S = 105\ k_B$/baryon, the initial velocity of the *r*-process material was 2000 km/s, and its initial radius was 10 km. The initial seed was 50% ^{70}Fe.

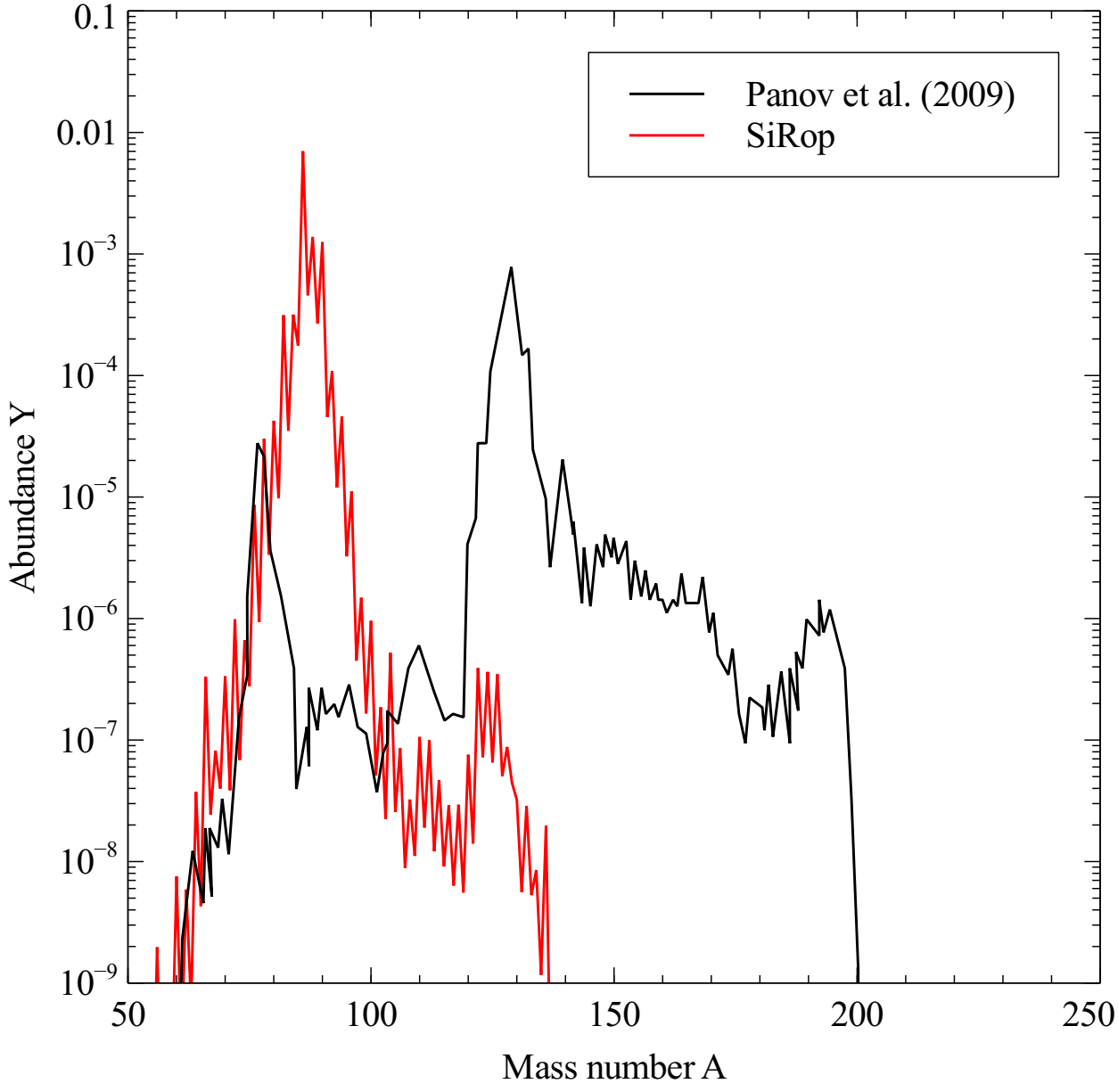

Figure 3.5: Comparison of *r*-process simulation results between those generated in SiRop and those from Panov et al. (2009) [23]. The simulations were run in a HEW *r*-process environment with initial temperature $T_9^0 = 2$, initial electron fraction $Y_e = 0.42$, and an expansion timescale $\tau = 0.005$ s. As well, the initial entropy $S = 105\ k_B$/baryon, the initial velocity of the *r*-process material was 2000 km/s, and its initial radius was 10 km. Nuclear statistical equilibrium (NSE) was run prior to this simulation, and the initial seed was 1% protons and 99% neutrons.

Parameters	Network	$\rho(t)$	entropy (k_B/baryon)
Aprahamian et al. (2014)	Full	Panov et al. (2009)'s evolution	3305
SiRop	WPA	Default	N/A

Table 3.6: Table of parameters (continued).

where $\rho_1 + \rho_2$ is the density at $t = 0$, τ is proportional to the expansion timescale, and Δ was chosen such that the two terms on the right-hand side would be equal at $T_9 = 2$ (the simulations began at $T_9^0 \approx 6$). This model simulates *r*-process material that expands exponentially before evolving to a constant-velocity outflow. I was unable to run the simulation with this particular density evolution; to address these and implement this density evolution would be useful to do in the future.

All in all, the efforts to recreate these other studies were unsuccessful. However, they hint at a larger problem with comparing sensitivity studies. In the following sections we will discuss these inconsistencies with regards to sensitivity metrics and normalization; indeed the issue with initial conditions is somewhat beyond the scope of this thesis (a more broad look at this problem is certainly worth pursuing). The difficulty in determining the initial conditions of a given study such that it can be meaningfully compared to another has the same implications as those with sensitivity study results, and is a much deeper concern.

Chapter 4

PAPER I: CRITICAL ASSESSMENT OF NUCLEAR SENSITIVITY METRICS FOR THE R-PROCESS

Carlton-James Osakwe, Nico Koning, Rachid Ouyed, Iris Dillmann, Reiner Krücken, and Prashanth Jaikumar

4.1 Foreword

I took over this paper from another student that left academia several years ago (namely Zachary Shand, who is referenced in [26] and [27]). The paper had been submitted, and revisions had been requested by the referee. I started my project addressing the revisions requested by the referee, the biggest requests being expanding the range of isotopes studied analyzing how the sensitivity measures were affected by neutron freeze-out (which occurs when there are no longer enough free neutrons for the *r*-process to continue). These revisions, as well as future correspondence with the referees, were the primary motivation of Section 3.1 (as an example, the referees pointed out the initial discrepancy between my numbers and the numbers in the original paper). This paper is currently under revision again after being re-submitted in July 2020.

4.2 Abstract

Any simulation of the *r*-process is affected by uncertainties in our knowledge of nuclear physics quantities and astrophysical conditions. It is common to quantify the impact of uncertainties in individual pieces of nuclear data on the r-process abundance pattern through a global sensitivity metric, which is then used to identify specific nuclides that would be most worthwhile to measure experimentally. Using descriptive statistics, we assess a set of metrics used in previous sensitivity

studies, as well as a new logarithmic measure. For certain neutron-rich nuclides lying near the *r*-process path for the typical hot-wind scenario, we find varying conclusions on their relative sensitivity implied by different metrics, although they all generally agree on the most sensitive nuclei. Part of the reason is that sensitivity metrics which simply sum over variations in the *r*-process distribution depend on the scaling used in the baseline, which often varies between simulations. We show that normalization of the abundances causes changes in the reported sensitivity factors and recommend reporting a minimized F statistic in addition to a scale estimation for rough calibration to be used when comparing tables of sensitivity factors from different studies.

4.3 Introduction

About half of all the stable nuclei heavier than iron are produced by the *r*-process [3, 4], which occurs in explosive neutron-rich astrophysical environments. Parameterized studies of neutron-rich flows and a growing set of observations from metal-poor stars suggest that no proposed site can produce the entire *r*-process [24, 28]. For a complete understanding of the origin of heavy elements, theoretical simulations of the *r*-process are essential in discriminating between the several proposed astrophysical sites, but are faced with modeling uncertainties in the nuclear physics inputs for neutron-rich nuclei. Rare-isotope measurements at existing and upcoming experimental facilities can reduce these uncertainties. This requires that key isotopes for the *r*-process in experimentally accessible regions of the nuclide chart are identified for measurements. To accomplish this, quantitative metrics, called "sensitivity factors", have been developed [2, 19, 20].

Nuclear mass models are crucial to the *r*-process, since they affect neutron separation energies (S_n), β-decay Q-values (Q_β), β-decay half-lives ($T_{1/2}$), neutron-capture cross sections, etc., which are all important input parameters to a full network calculation. Even in the classical waiting-point approximation (WPA), the use of different nuclear mass models with variations in the predicted shell structure near the magic numbers alters S_n (i.e. the *r*-process path) and the final calculated abundance [20]. Although we will not achieve a complete measured range up to the drip line, as

the number of experimentally measured masses increases we can hope that the predictive power of the nuclear mass models will improve [14, 29].

To quantify how the uncertainty in nuclear properties propagates to the *r*-process abundance pattern, a global sensitivity measure (or "impact parameter") F is utilized in some studies, which is examined in detail in this paper (see [2, 19, 20] for various definitions of F). Based on this metric, key pieces of data are identified near the neutron closed shells and the precursors of the rare-earth peak which are most influential in generating the overall abundance pattern [31]. While this metric, and its variations in the series of papers on sensitivity studies (see Ref. [21] for a review), is a simple way to capture the impact of variations in the nuclear parameters (locally or globally), distilling the sensitivity to a single number is potentially fraught with erroneous conclusions on the relative importance of some isotopes, as we demonstrate in this paper. The freedom to scale or normalize the simulated *r*-process pattern in an arbitrary way can also lead to differing conclusions on the sensitivity depending on the metric used.

The purpose of this work is two-fold: (i) to show that application of the existing metrics can lead to varying conclusions on the relative importance of certain nuclides in producing the best fit to the *r*-process abundance pattern; (ii) to introduce a statistical significance to the F-metric that takes the arbitrariness in baseline normalization into account, so that conclusions on the sensitivity are more refined and specific to the metric used.

The paper is organized as follows: In Sec. 4.4, we set up our *r*-process waiting-point simulation with the SiRop code[1] and calculate the variations in the abundance using different measures due to changes in the theoretically predicted nuclear mass. In Sec. 4.5, we compare the performance of four different metrics and highlight differing conclusions on the sensitivity of the *r*-process pattern to nuclear masses around the A=130 peak. In Sec. 4.6, we describe the effect of scaling and normalization, followed by our conclusions in Sec. 4.7.

[1] `http://www.quarknova.ca/SiRop/`

4.4 Simulation Parameters

We generate our *r*-process simulation data using an extension of the r-Java 2.0 code [12] that now includes a graphical-user interface (GUI) module for sensitivity runs. This first-of-its-kind code, "SiRop", allows users to run the *r*-process simulation and output sensitivity metrics in a single Java-based application in order to represent and analyze changes in the abundance curves. The data used to compare the sensitivity studies was computed in the WPA for fast computation of data to test and compare each metric. The results of the baseline and varied simulations is shown in the top panel of Fig. 4.1. For the baseline, we used a parametric trajectory for the density of $\rho = \frac{\rho_0}{(1+t/2\tau)^2}$ where $\rho_0 = 10^{11}$ g cm^{-3} and the expansion timescale $\tau = 0.01$ s, and an initial temperature of $T = 3 \times 10^9$ K. The trajectory ensures validity of the WPA and production of *r*-process elements including the third peak at $A = 195$.

The initial isotopic composition of the environment was set to 50% ^{70}Fe by mass (i.e. $X_{70\mathrm{Fe}} = 0.5$) corresponding to an initial neutron-to-seed ratio of 62. The code was run until this ratio dropped below one at which point the temperature and neutron number density of the simulation were 2.7×10^9 K and 4.6×10^{28} cm^{-3}, respectively. These values were used to calculate the waiting point population coefficients (WPPC) displayed in Fig. 4.2 as circles. The varied simulations consisted of changes in masses of single isotopes in a grid spanning from ^{128}Cd to ^{139}Te. These isotopes were chosen as they are in the predicted *r*-process path and match the isotopes selected in [30]. Additional computations were done on selected low-abundance isotopes from other regions of the nuclear chart for completeness (the computed sensitivity factors are shown in Table 4.1). For each isotope, the simulation was run twice, simulating both a decrease and an increase in the isotope's mass by 0.0005%, corresponding to a change of approximately ± 0.6 MeV. This value represents the average deviation of mass models from known experimental values.

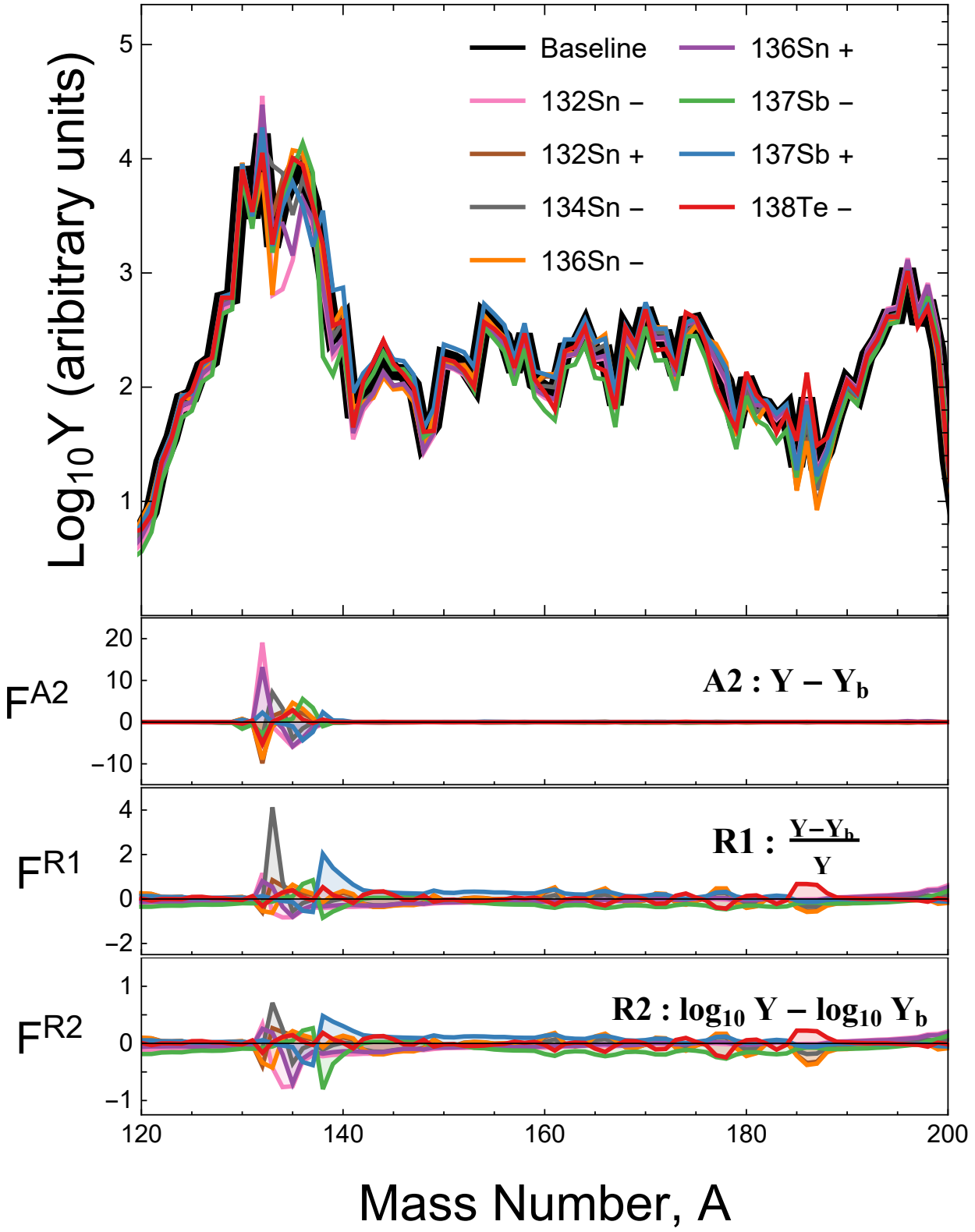

Figure 4.1: Abundance pattern in the *r*-process simulation showing baseline vs eight most sensitive mass changes (labels indicate isotope's mass was decreased or increased by 0.0005%). The lower three panels show the deviation from the baseline as defined by the metrics listed in Sec. 4.5. The top shows metric A2 (units of mass normalized abundance multiplied by 10^4), the middle shows metric R1 (unitless) and the bottom shows metric R2 (unitless). Metric A1 is not shown because it is identical to metric A2, save for a weighting by mass number.

4.5 Metric performance comparison

Both global and local sensitivity metrics have been used in other works (e.g. [2, 19, 20]), with global sensitivity metrics (sums of variations over mass numbers) providing a convenient and digestible value which can be used to estimate the total variation induced by a changing nuclear parameter (or set of parameter changes). This number alone, however, provides no description of how the abundances changed. For example, a large overproduction of a single isotope is indistinguishable from many equivalent differences distributed over many isotopes. We test four different definitions of the metric. The fourth is newly introduced in this work:

- A1: absolute mass fraction difference $|\mathrm{X\text{-}X_{base}}| = |\mathrm{A(Y\text{-}Y_{base})}|$
- A2: an abundance difference $|\mathrm{Y\text{-}Y_{base}}|$
- R1: a relative difference $|\frac{\mathrm{Y}-\mathrm{Y_{base}}}{\mathrm{Y_{base}}}|$
- R2: a log-ratio $|\log_{10}\frac{\mathrm{Y}}{\mathrm{Y_{base}}}| = |\log_{10}\mathrm{Y} - \log_{10}\mathrm{Y_{base}}|$.

In the case of the given metrics, the corresponding sensitivity factor F_i^M (for a metric M and an increase or decrease in the mass of nuclide i) is given by $F_i^M = \sum_{N,Z} M$. For metrics R1 and R2 the use of mass fractions or abundances is interchangeable as the factor of A ($X = A \cdot Y$) cancels out in the ratio.

Metrics A1 and A2 overweight changes at or near the peaks in the *r*-process distribution due to the order of magnitude differences between isotope abundances. They are also more sensitive to an overproduction of isotopes. In contrast, R1 and R2 do not overemphasize changes in the more abundant isotopes, which is useful when examining the details of the abundance distribution. Both R1 and R2 produce similar results when the changes in ratio or percentages are small, because the series expansion to first order of the log-ratio is identical (within a constant) to the relative difference.

Application of these metrics to the simulated data shows that each metric has varying sensitivity to the mass variations in our study. It is apparent from Fig. 4.2 that the four metrics have

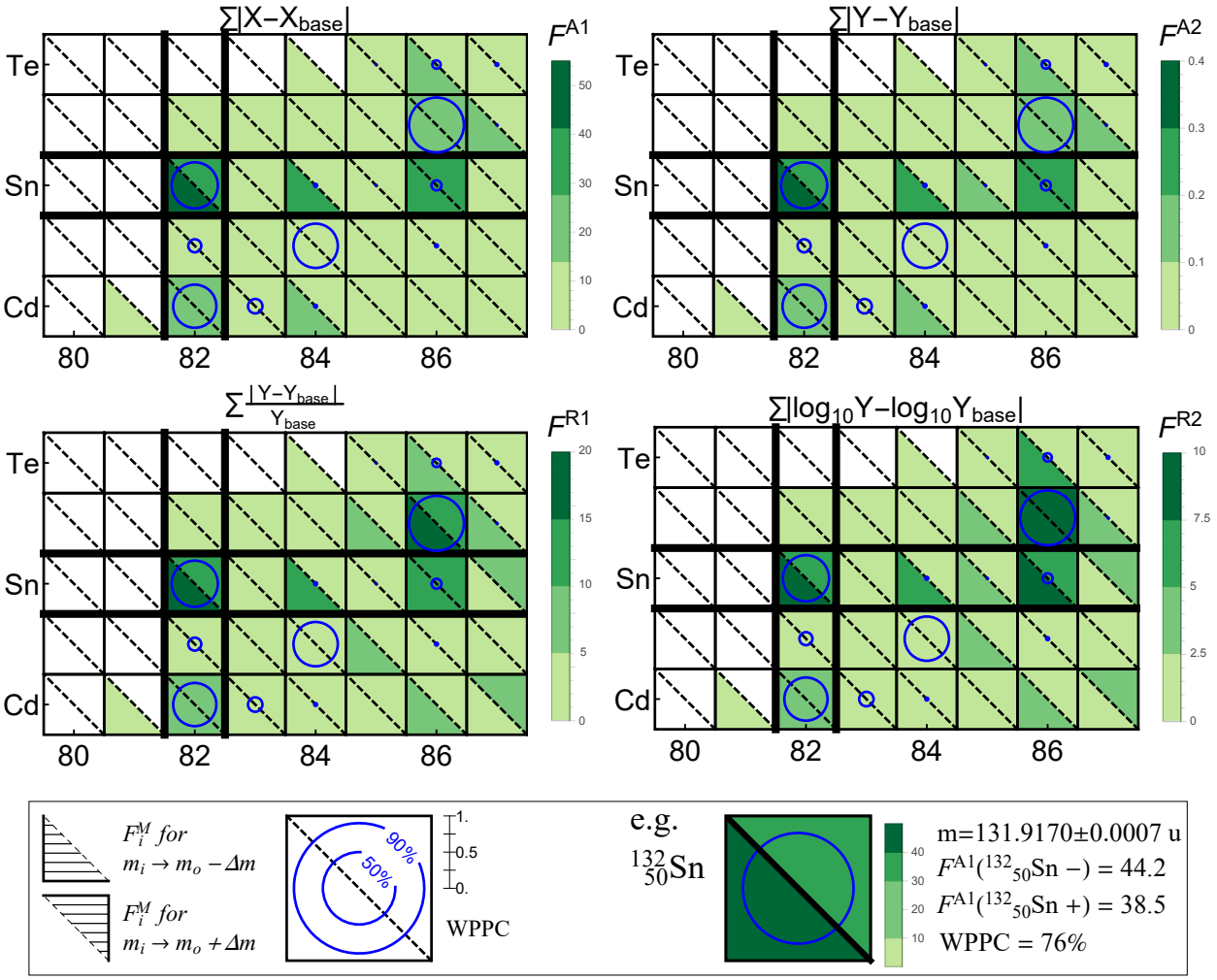

Figure 4.2: The calculated sensitivity factor (F_i^M) for each metric is color coded as shown in the legend. The sensitivity factor calculated after decreasing the mass of one isotope is plotted in the bottom left of the isotope in the chart. The increase in mass is on the top right triangle. The circles indicate the *r*-process waiting point population coefficients (WPPC) as determined by the nuclear Saha equation. The diameter is proportional to the population coefficient (the full height of each square corresponds to 100%, and no circle indicates a population of approximately 0%). The sensitivity over the mass range $120 \leq A \leq 200$ is calculated using mass fraction normalized abundances. The results have been both normalized and calibrated, as defined in Sec. 4.6.
Even for our small test study we see that the metrics disagree both qualitatively and quantitatively.

very different numerical values as expected, but significantly, they do not necessarily agree on the relative sensitivities of different isotopes. A1 and A2 favor the most abundant isotope ^{132}Sn[2] and indicate higher sensitivity to the mass of ^{132}Sn being decreased by 600 keV rather than increased by the same amount. In contrast, R1 and R2 assess ^{137}Sb as the most sensitive isotope and indicate nearly identical sensitivities for the increase and decrease in the mass of ^{132}Sn. The differences are most apparent for the $N = 86$ isotopes, in particular ^{137}Sb, for which only R1 and R2 show high sensitivity. Just from looking at metrics A1 and A2 an experimentalist might focus on ^{132,134,136}Sn whereas looking at R2 would shift that focus to ^{132,136}Sn and ^{137}Sb. It should be noted that ^{133}In is shown to have low sensitivity despite being highly populated. This is because the S_n from FRDM used for ^{134}In fits the Saha equation for $n_n = 4.6 \times 10^{28}$ cm^{-3} and $T = 2.7 \times 10^9$ K better than the S_n for ^{132}In. Metrics A1 and A2 are identical except for a weighting by mass number present in A1 which will cause the two to perform differently when comparing changes near the first, second, and third abundance peaks.

For our test data, R1 and R2 perform almost identically; however, R1 emphasizes overproduction of isotopes which had smaller abundances in the baseline (see ^{134}Sn and ^{137}Te in Fig. 4.2 and Fig. 4.1) while R2 responds equally to under- and over-production by a constant factor (e.g. twice the abundance vs. half the abundance).

In Fig. 4.1 we see that the exponential sensitivity of the WPA (S_{1n}) leads to large changes to the abundances. While metric A2 (Y-Y$_b$) seems to imply that large changes only occur in the neighborhood of the nuclide whose mass was altered, the relative metrics (R1,R2) (bottom two panels in Fig. 4.1) magnify changes in low-abundance nuclides, showing that there are also large effects on heavier nuclides. Changes to some isotopic masses (like ^{134}Sn) cause strong local variation in the simulated abundances, while others (like ^{137}Sb) only produce changes to the abundance of several isobars. In calculating a global sensitivity factor F we lose information about the details of the differences in the data, but simplify the interpretation and presentation of the calculated sensitivity.

[2]Normally ^{130}Cd is expected as the most abundant isotope in our region of interest as the precursor to the $A = 130$ peak; however, in our test data set the WPA strongly favoured ^{132}Sn at freeze-out conditions.

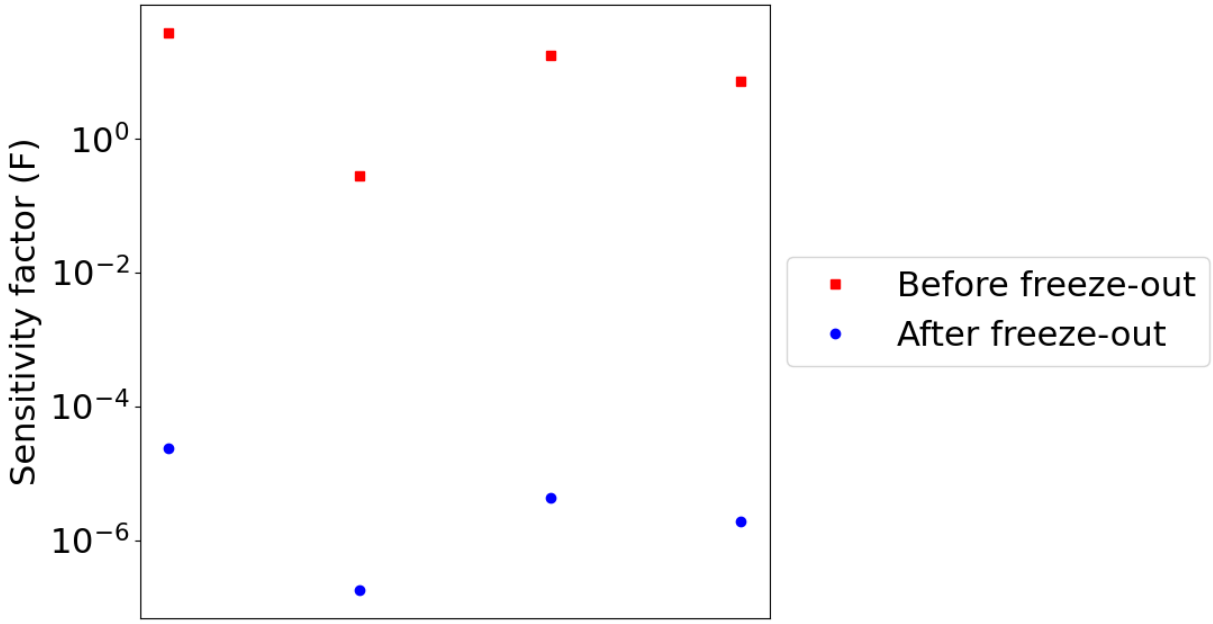

Figure 4.3: Sensitivity computed for ^{132}Sn using the waiting point approximation and a full-network simulation including the freeze-out phase. The mass of each isotope was increased by 0.0005%; the data for the figure is from Table 4.2.

With regards to the tests on other low-abundance isotopes in the abundance pattern, metrics R1 and R2 consistently assessed these isotopes to be more sensitive relative to metrics A1 and A2. This would suggest that R1 and R2 overemphasize changes in lower-abundance isotopes.

4.5.1 Sensitivity beyond freeze-out

Full-network simulations were also run in order to analyze the behaviour of the sensitivity metrics after the freeze-out phase. The results (shown in Table 4.2 and Figure 4.3) show the mass sensitivity of ^{132}Sn decreasing by factors of 10^6 - 10^7 across metrics A1, A2, and R1, with increases by factors of 10^5 - 10^6 for R2. This suggests that the complexity of the freeze-out phase depresses sensitivity values regardless of metric used. This complexity could be explored in greater detail in a future work.

The best choice of metric seems unclear and depends on what type of changes in the *r*-process distribution are of interest. For large scale variations like the type shown in the test data here, it seems like the log-ratio R2 performs best; however, different changes in the nuclear parameters do not necessarily provoke such strong variations. Changes in the β-delayed branching ratios, for example, are likely to only cause small local changes during freeze-out, and in this instance A2 could be the best metric for studying these nuclear parameters. Due to these potential disagreements and differences in sensitivity of the metrics, we caution against placing too much weight on any single global sensitivity metric.

4.6 Normalization and Calibration

4.6.1 Normalization

The *r*-process is a set of abundance values which are important in aggregate as a relative distribution and, without an astrophysical context, the absolute abundances are arbitrary up to a positive multiplicative constant. When observationally available, these relative abundances are consistent with the solar *r*-process residuals ($\mathrm{N}_r = \mathrm{N}_\odot - \mathrm{N}_s - \mathrm{N}_p$, this equation describes how we extract the abundance yields of the *r*-process from solar abundance data, which includes abundances from the *s*-process and *rp*-process; the *rp*-process is like the *r*-process, but it is based around proton capture and β^+-decay) [28]. In principle, a good agreement of a single simulation does not say anything; one has to run hundreds of simulations with varying astrophysical input parameters (metallicity, stellar masses, sites, etc.) and then see the solar *r*-process abundances as a superposition of these values. Observations are normalized to Ba for (*s*-process) or Eu (*r*-process), but simulated data from a single calculation is typically normalized by mass fraction. For this reason, comparing theoretical calculations to observational data or other simulation data is not so straightforward. In order to then calculate the sensitivity value we need to somehow normalize our simulated abundances before calculating how sensitive the *r*-process is to the underpinning nuclear parameter we have varied. If we had information about an underlying probability distribution for the *r*-process

abundances it would be more obvious how to compare the two sets of data (e.g. χ^2 or other maximum likelihood methods). However, the sparsity of observational data, long simulation times, and large variability in abundances from simulations preclude many standard statistical methods. For these reasons, we are forced to rely on these simple tests to estimate which inputs caused the largest or most significant variation. This is possible only if we can meaningfully interpret the numerical values computed for our sensitivity factors and ensure that the methods for determining relative sensitivities are properly normalized and consistent.

In order to clarify what we mean by this, we first re-write the sensitivity metrics with two arbitrary scaling constants a and b as follows:

$$F_i^{A1} = \sum_{N,Z} |aX_i - bX_b| = \sum_{N,Z} b \left| \frac{a}{b} X_i - X_b \right| \tag{4.1}$$

$$F_i^{A2} = \sum_{N,Z} |aY_i - bY_b| = \sum_{N,Z} b \left| \frac{a}{b} Y_i - Y_b \right| \tag{4.2}$$

$$F_i^{R1} = \sum_{N,Z} \left| \frac{aY_i - bY_b}{bY_b} \right| = \sum_{N,Z} \left| \frac{\frac{a}{b} Y_i - Y_b}{Y_b} \right| \tag{4.3}$$

$$F_i^{R2} = \sum_{N,Z} \left| \log_{10} \frac{aY_i}{bY_b} \right| = \sum_{N,Z} \left| \log_{10} \frac{a}{b} Y_i - \log_{10} Y_b \right|, \tag{4.4}$$

where Y_b is the baseline abundances and Y_i is the abundance data with our i$^{\text{th}}$ varied set of nuclear parameters. In each metric we can identify the term $\frac{a}{b} Y_i$ which indicates that when comparing Y_i to Y_b we can find constants a, b which minimize F. We refer to solving for the constant a/b which minimizes the computed sensitivity factor F as normalization. For our test data, we show the change to the final reported value for the most sensitive values (after normalization) for each metric in Table 4.3.

The normalization procedure does not vary most values by more than a few percent for any of the metrics, but in the test data here the variation can be as much as 39%. However, we do see differences which have the potential to become more pronounced when applied to either more comprehensive or more complex studies. In cases where there is significant non-local change, nor-

malization is expected to show more significant corrections to the sensitivity factors and will allow for more robust measures of these changes. The computational simplicity makes it a reasonable and prudent improvement to the existing method for computing sensitivity factors.

4.6.2 Calibration

When writing the sensitivity factors with normalization constants, we have also explicitly exposed another potential ambiguity in interpreting and comparing metrics defined using simple differences of abundances (or mass fractions). In equations 4.1 and 4.2 the factoring process exposed a scale parameter b which pre-multiplies the metric. (Equations 4.3 and 4.4 in contrast are purely relative or scale-free.) Given that our relative abundance data is of arbitrary magnitude, differences in implicit scale (b) will cause these type of metrics to report different absolute magnitudes for sensitivity depending on how they happen to have been scaled. If the data is reported by an r-process code which relies on mass fraction normalization (e.g. r-Java 2.0) then we would expect the 2$^{\text{nd}}$ r-process peak to have an abundance of Y$\sim 10^{-3}$. Local changes in the peak will (for these difference type metrics) swamp out any non-local changes and the sensitivity factor F will be close to 10^{-3}. The values we have reported in Table 4.4 were computed after multiplying our abundances by a factor of 100 (this has the effect of making our definition of F^{A1} in Eq. 4.1 consistent with the definition in [20]) and as expected, the reported values for F^{A1} and F^{A2} are the same order of magnitude as the maximum abundance ($F^{A1} \sim A_{\max} \cdot Y_{\max} = 32.6$ and $F^{A2} \sim Y_{\max} = 0.247$) as indicated at the bottom of Table 4.4. For this reason, we recommend that sensitivity factors be reported with the peak abundance as we have done at the bottom of Table 4.4. The maximum abundance in the baseline, while not a perfect indicator, can assist in comparison of studies. We refer to this technique as "calibration" and it will allow comparison of sensitivity values from different studies with different baselines.

4.7 Conclusion

We have performed sensitivity studies of the *r*-process to assess a few different global sensitivity metrics that have been proposed in recent work. While some of the biases and limitations of the metrics have been mentioned before, this is the first work that compares its various definitions by applying them on a single simulation. Besides showing that metrics of the form presented in this work can give different results on the relative sensitivity of certain nuclides that lie on or near the *r*-process path, we also demonstrated that normalization of the abundances can affect the computed sensitivity. Computations done in the rare earth element region were also performed (but not presented here) which confirm the preferential bias of metrics A1 and A2 for higher sensitivity near the abundance peaks. In addition, we presented a technique for calibrating sensitivity values from different studies.

Based on our findings of variations from one metric to another, we do not recommend their use as the only analysis tool for sensitivity. Ideally, one should understand the particular response of each metric definition, but computation of all metrics simultaneously (and any others that seem reasonable) seems prudent. We also recommend that the abundance distributions be normalized in some fashion and recommend reporting a minimized F. When reporting metrics F^{A1} or F^{A2}, maximum abundance information should be provided to assist in calibration and comparison of different sensitivity studies. These recommendations are aimed at improving the strength of sensitivity studies using global sensitivity factors and are designed to allow for more robust statistical inference from *r*-process simulations.

Z	A	A1+	A2+	R1+	R2+
85	213	1.71	0.012	1.68	0.734
46	88	1.36×10^{-12}	9.75×10^{-15}	1.14×10^{-12}	4.95×10^{-13}
30	95	0.844	0.006	0.801	0.348
50	140	0.299	0.002	0.241	0.105
55	185	8.79×10^{-10}	6.44×10^{-12}	6.80×10^{-10}	2.95×10^{-10}
Z	A	A1-	A2-	R1-	R2-
85	213	0.967	0.007	0.952	0.415
46	88	1.36×10^{-12}	9.74×10^{-15}	1.13×10^{-12}	4.89×10^{-13}
30	95	0.141	0.001	0.181	0.079
50	140	0.896	0.007	0.765	0.335
55	185	1.29×10^{-9}	9.43×10^{-12}	9.98×10^{-10}	4.33×10^{-10}

Table 4.1: Additional sensitivity factors computed for selected isotopes in other regions of the nuclear chart. These were calculated using the metrics defined in the manuscript. The + and - signs indicate that the mass of each isotope was increased or decreased by 0.0005%, respectively.

	A1+	A2+	R1+	R2+
Waiting point	37.9	0.277	17.4	7.24
Full-network	2.34×10^{-5}	1.77×10^{-7}	4.34×10^{-6}	1.89×10^{-6}
	A1-	A2-	R1-	R2-
Waiting point	40.7	0.287	14.7	7.26
Full-network	2.34×10^{-5}	1.77×10^{-7}	4.34×10^{-6}	1.89×10^{-6}

Table 4.2: Sensitivity computed for ^{132}Sn using the waiting point approximation and a full-network simulation including the freeze-out phase. The + and - signs in the legend indicate that the mass of each isotope was increased or decreased by 0.0005%, respectively.

		F_{default}	F_{min}	ΔF (%)	a/b
	^{132}Sn−	53.6	50.7	-5.4	0.70
	^{136}Sn+	40.2	39.3	-2.2	0.85
F^{A1}	^{134}Sn−	29.0	28.6	-1.5	1.03
	^{136}Sn−	31.1	28.1	-9.6	0.81
	^{137}Sb−	26.9	26.9	-0.0	0.97
	^{132}Sn−	0.396	0.366	-7.5	0.46
	^{136}Sn+	0.296	0.289	-2.3	0.82
F^{A2}	^{134}Sn−	0.214	0.210	-1.6	1.03
	^{136}Sn−	0.228	0.203	-11.0	0.81
	^{132}Sn+	0.223	0.194	-12.8	0.84
	^{136}Sn−	16.0	16.0	-0.0	1.00
	^{132}Sn+	14.9	14.9	-0.2	0.98
F^{R1}	^{137}Sb−	20.0	14.7	-26.5	1.24
	^{132}Sn−	15.7	14.7	-6.7	1.09
	^{134}Sn−	14.0	13.5	-3.5	1.04
	^{136}Sn−	7.43	7.27	-2.3	1.05
	^{132}Sn−	8.15	6.99	-14.2	1.15
F^{R2}	^{132}Sn+	6.73	6.61	-1.7	1.05
	^{137}Sb−	10.3	6.32	-38.8	1.31
	^{137}Sb+	6.74	5.57	-17.4	0.89

Table 4.3: Sensitivity factors reported using a default scaling/normalization constant ($a/b = 1.0$) compared to the sensitivity factors minimized using different scaling constants a/b. The blocks consist of the top five rated isotopic changes (after minimization). The columns list from left to right: the isotope whose mass was changed (here + or - indicate an increase or decrease of 600 keV, respectively), the default sensitivity value, the minimal sensitivity factor, the percent difference, and the scaling constant which minimized the F value.

	F^{A1}	F^{A2}	F^{R1}	F^{R2}
^{130}Cd−	18.4	0.137	7.3	3.23
^{130}Cd+	17.5	0.130	7.2	3.13
^{131}Cd−	10.7	0.081	3.2	1.38
^{132}Cd+	11.9	0.089	3.2	1.52
^{135}Cd+	10.9	0.080	6.7	2.86
^{134}In−	10.3	0.075	6.2	2.66
^{132}Sn−	<u>50.7</u>	<u>0.366</u>	14.7	<u>6.99</u>
^{132}Sn+	26.7	0.194	<u>14.9</u>	<u>6.61</u>
^{134}Sn−	<u>28.6</u>	<u>0.210</u>	13.5	4.73
^{135}Sn−	12.4	0.091	3.9	1.50
^{136}Sn−	28.1	0.203	<u>15.9</u>	<u>7.27</u>
^{136}Sn+	<u>39.3</u>	<u>0.289</u>	11.4	5.11
^{137}Sn+	11.6	0.085	7.1	3.04
^{136}Sb−	11.0	0.080	6.4	2.73
^{137}Sb−	26.9	0.193	<u>14.7</u>	6.32
^{137}Sb+	20.6	0.147	13.3	5.57
^{138}Sb−	13.6	0.099	9.4	3.91
^{138}Te−	17.4	0.127	10.6	4.51

Range: $120 \leq A \leq 200$

$Y_{\max} = 0.247$ at $A = 132$

Table 4.4: Summary of global sensitivity factors computed based on different statistical metrics. The isotopes and sensitivity factors reported in the table are a combination of the top 15 most sensitive isotopes according to each metric. The top three most sensitive isotope mass changes are underlined in each column. These sensitivity values have been computed after normalization (i.e. $F^a_{\min}$) according to each respective metric.

Chapter 5

PAPER II: NORMALIZATION AND CALIBRATION OF R-PROCESS NUCLEAR SENSITIVITY METRICS

Carlton-James Osakwe, Nico Koning, and Rachid Ouyed

5.1 Foreword

This paper aims to expand on the point in Section 4 regarding normalization. It looks at how normalization can affect sensitivity, such that we can standardize the normalization of sensitivity study results (in a manner analogous to how the previous paper looks at sensitivity metrics). I wrote this paper in its entirety; the paper is complete but is yet to be submitted.

5.2 Abstract

We discuss the importance of normalization when reporting on the r-process sensitivity of nuclear isotopes. Four different sensitivity metrics are used in this analysis. We conclude that normalizing results so as to minimize the sensitivity factor F is a desirable standard for future studies, and that this will be the case in general, independently of the r-process code or network used. We also conclude that sensitivity metrics that use relative differences in abundance are preferable to those using absolute differences when it comes to normalization, as the former are shown to eliminate arbitrary scaling factors that are otherwise introduced.

5.3 Introduction

The r-process is responsible for about half of the abundance of heavy elements in the universe [3, 4]. Most of the nuclei involved are exotic, neutron-rich species whose properties have not been

directly measured. We use nuclear models (e.g., FRDM, HFB-21) to predict their properties in simulations; these generally all predict the properties of nuclei we have measured, but disagree somewhat when it comes to more exotic nuclei. There is therefore an interest in identifying which nuclei are most important in the *r*-process, that we may prioritize them for measurement in experimental facilities [1].

To identify these nuclei, we have conducted sensitivity studies [27]. These studies use small changes in input parameters (to represent the differences between nuclear models) in *r*-process simulations and measure the differences in the results. Those differences quantify the importance of each isotope (known as the "sensitivity") with respect to the input parameter being varied (e.g., mass, reaction rates). We then use what are called sensitivity metrics to convert these differences into numbers (called sensitivity factors, denoted by F) that can be compared.

Comparing sensitivity studies to each other or to observational data is complicated by the fact that there is no consistent way to normalize sensitivity study results. Observational *r*-process data are typically normalized to Eu, but simulation results are, in general, normalized by mass fraction. It would therefore be useful to find a consistent method of normalization for these studies. As well, this in-depth study of normalization and its effects on *r*-process simulation results may in itself yield useful information about sensitivity.

5.4 Initial parameters

For this study of sensitivity factor normalization we used the SiRop *r*-process simulation code[1] [26]. This code produces *r*-process abundance patterns with double-precision computation. SiRop can simulate a variety of astrophysical environments, including high-entropy winds from proto-neutron stars, neutron star mergers, and quark novae. We used a custom *r*-process environment (as described in [17]) in our study that had an initial density $\rho_0 = 10^{11}$ g cm^{-3}, an expansion timescale of $\tau = 0.01$ s, an initial electron fraction $Y_e = 0.3$, and an initial temperature $T_0 = 3 \times 10^9$

[1] http://www.quarknova.ca/SiRop/

K. The density evolved in time as $\rho(t) = \frac{\rho_0}{(1+t/2\tau)^2}$. The initial seed was set to 50% ^{70}Fe (i.e. the initial mass fraction X_0 of ^{70}Fe was 0.5), and the simulation was run until the neutron-to-seed ratio dropped below one. As well, this analysis uses the waiting point approximation (WPA) [5]. For the sensitivity studies, we looked at five isotopes in the *r*-process chain, namely ^{132}Sn, ^{128}Cd, ^{135}Te, ^{140}Sn, and ^{137}Sb. These isotopes were selected as a sample of the isotopes whose sensitivity was assessed in the work of which this paper is a continuation [27]. The mass of each isotope was varied by 0.0005%.

The sensitivity metrics we looked at are as follows:

$$\begin{aligned} F^{A1} &= \sum_{N,Z} |X - X_{\text{base}}| \\ F^{A2} &= \sum_{N,Z} |Y - Y_{\text{base}}| \\ F^{R1} &= \sum_{N,Z} \left| \frac{Y - Y_{\text{base}}}{Y_{\text{base}}} \right| \\ F^{R2} &= \sum_{N,Z} \left| \log_{10} \frac{Y}{Y_{\text{base}}} \right| \end{aligned} \tag{5.1}$$

Here the sums are over neutron number N and proton number Z for every isotope in the resultant abundance pattern. X is the mass fraction, and Y is the abundance. X_{base} and Y_{base} refer to the mass fraction and abundance of the control (or baseline) *r*-process simulation, respectively. Metrics A1 and A2 are based on absolute differences between abundance patterns, while R1 and R2 are based on relative differences. The first two metrics place more importance on differences between isotopes with smaller absolute abundances than the latter two; for a more detailed discussion see [27].

We know that the sensitivity factor F can be minimized because, for a given set of abundance patterns (the baseline and one where the mass of one isotope was changed, for example), there must exist a scaling factor that, when applied to one of the patterns, will make the two patterns maximally similar. This scaling factor would therefore minimize the sensitivity factor F. Figure 5.1 shows an illustration of this principle. Of course, for isotopes with low sensitivity, this scaling

factor will be close to one, since in that case the abundance pattern will already be similar to the baseline. Isotopes with higher sensitivity will allow for a broader range of possible minimizing normalization factors. To recreate different normalizations for sensitivity study results, we applied two arbitrary scaling constants a and b to the aforementioned metrics as such:

$$\begin{aligned} F^{A1} &= \sum_{N,Z} |aX - bX_{\text{base}}| = \sum_{N,Z} b \left| \frac{a}{b} X - X_{\text{base}} \right| \\ F^{A2} &= \sum_{N,Z} |aY - bY_{\text{base}}| = \sum_{N,Z} b \left| \frac{a}{b} Y - Y_{\text{base}} \right| \\ F^{R1} &= \sum_{N,Z} \left| \frac{aY - bY_{\text{base}}}{bY_{\text{base}}} \right| = \sum_{N,Z} \left| \frac{\frac{a}{b} Y - Y_{\text{base}}}{Y_{\text{base}}} \right| \\ F^{R2} &= \sum_{N,Z} \left| \log_{10} \frac{aY}{bY_{\text{base}}} \right| = \sum_{N,Z} \left| \log_{10} \frac{a}{b} Y - \log_{10} Y_{\text{base}} \right| \end{aligned} \tag{5.2}$$

To study the effects of normalization, we varied the ratio a/b between 0.25 and 6 for the five isotopes mentioned before, in increments of 0.25. The data were fit with a cubic spline to obtain a general trend.

5.5 Results

We first sought to see how the four metrics mentioned earlier responded to changing normalization. Figure 5.2 shows a single isotope (^{132}Sn) where the sensitivity factor F was calculated for all four metrics. What is immediately noticeable is that the value of the normalization factor a/b that minimizes the sensitivity factor is different for each metric. This would suggest that the normalization of sensitivity study results as they relate to minimizing F is metric-dependent. As well, metrics A1 and A2 scale faster than R1 and R2 because the former two are absolute measures of sensitivity, while the latter two are relative.

When we apply our normalization constants a and b to metrics A1 and A2, an additional factor of b is introduced in the final sensitivity factor. The choice of b would presumably scale the results of any sensitivity study independently of the ratio a/b. In this work we set $b = 100$,

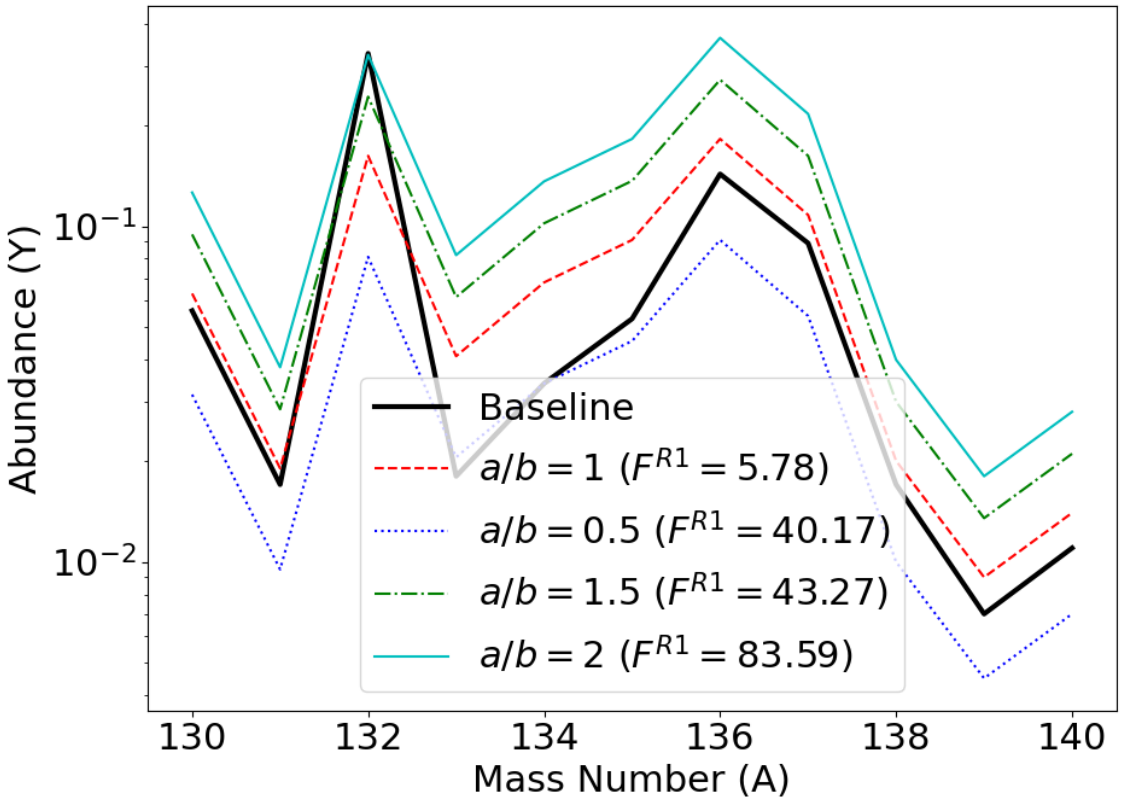

Figure 5.1: A slice of a set of abundance patterns from a sensitivity study of ^{132}Sn. The figure shows the baseline (control) simulation, as well as a simulation where the predicted mass of ^{132}Sn was increased by 0.0005%. The latter simulation is shown with several different normalization factors a/b with corresponding sensitivity factors F; there must exist a value of a/b that makes the latter simulation maximally similar to the former.

which made the definition of F^{A1} consistent with the definition in [20]. We refer to determining an appropriate scaling factor as calibration, this is also discussed in [27]. Some kind of indicator (e.g., the maximum abundance in the baseline simulation; a similar case was made in [27]) might then be necessary to compare different studies. Metrics R1 and R2 might then be preferable sensitivity measures to use, given that this stray scaling factor disappears when the constants are applied.

The minimized sensitivity factors for Figure 5.2 are displayed in Table 5.1. These minimized factors are also compared to their default values, where "default" is defined as having a normalization factor of one.

It was discovered in a previous work that different isotopes had their sensitivity factors minimized at different values of a/b [27]. We therefore looked at five different isotopes (^{128}Cd, ^{132}Sn, ^{140}Sn, ^{135}Te, and ^{137}Sb) and calculated their sensitivity factors using metric R2. The results are shown in Figures 5.3 and 5.4; it appears that the differences in sensitivity for the various isotopes are most pronounced when the results are normalized such that the factors are minimized.

As with Table 5.1, the minimized sensitivity factors for Figures 5.3 and 5.4 are displayed in Tables 5.2 and 5.3, respectively. We made the case in a previous work that normalizing sensitivity study results such that F is minimized would be a useful standard for normalization [27], and the analysis presented here suggests this as well. While we are able to make the case that the relative metrics are preferable to the absolute ones, it would be difficult to determine which of the relative metrics is superior without a broader study of isotopes. That said, one could say that metrics that minimize the sensitivity factor F at $a/b = 1$ for more isotopes may be better, since it will be less consequential if a given study does not normalize their results. In any case, this too would warrant a broader study in the future.

In this analysis we used the WPA for computational simplicity, but we expect that a full-network calculation would not significantly impact the main conclusion. The results originate directly from the normalization constants themselves (with regards to the minimization of sensitivity factor F and the arbitrary scaling introduced in to the absolute metrics); it follows that the

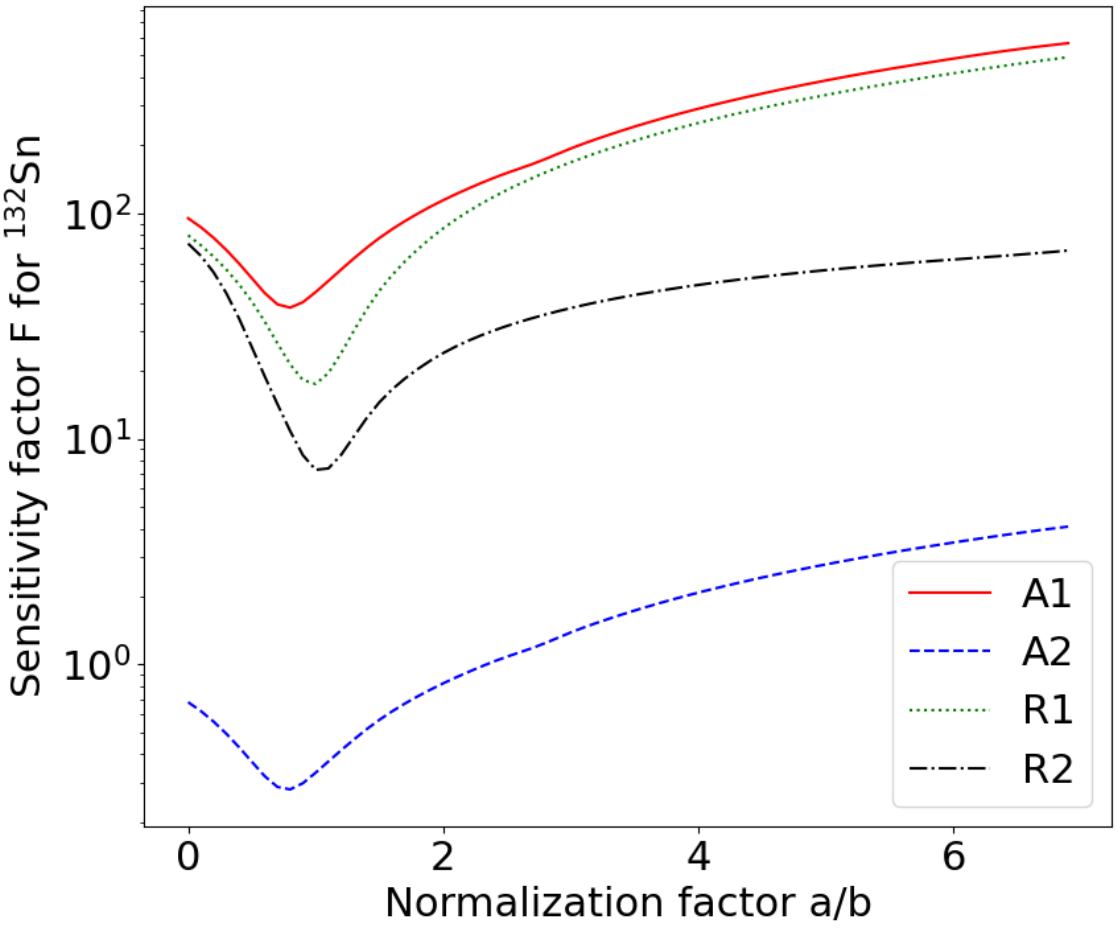

Figure 5.2: Comparison of sensitivity factors (for ^{132}Sn) as a function of normalization factor a/b for four different sensitivity metrics. The simulations were run in the custom r-process environment described in Section 5.4.

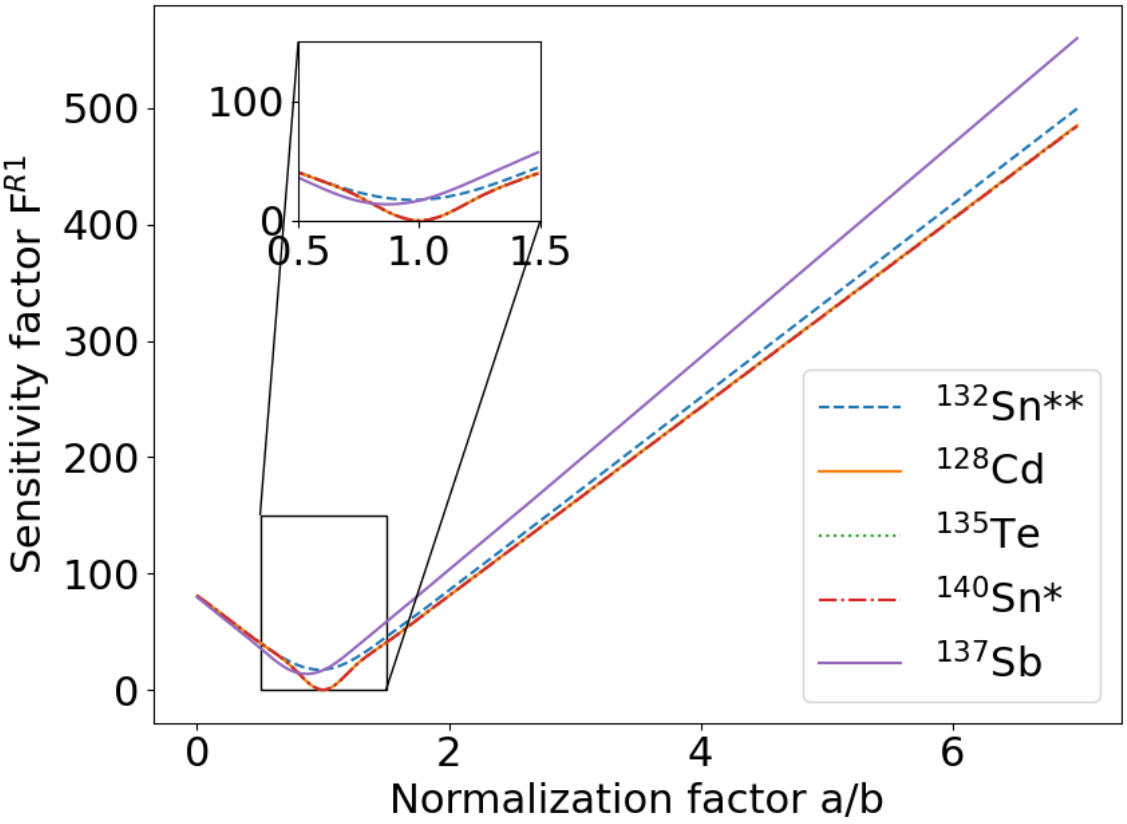

Figure 5.3: Comparison of sensitivity factors (using metric R1) as a function of normalization factor a/b for several different isotopes. The simulations were run in the custom r-process environment described in Section 5.4. The * indicates magic nuclei, and the ** indicates doubly-magic nuclei.

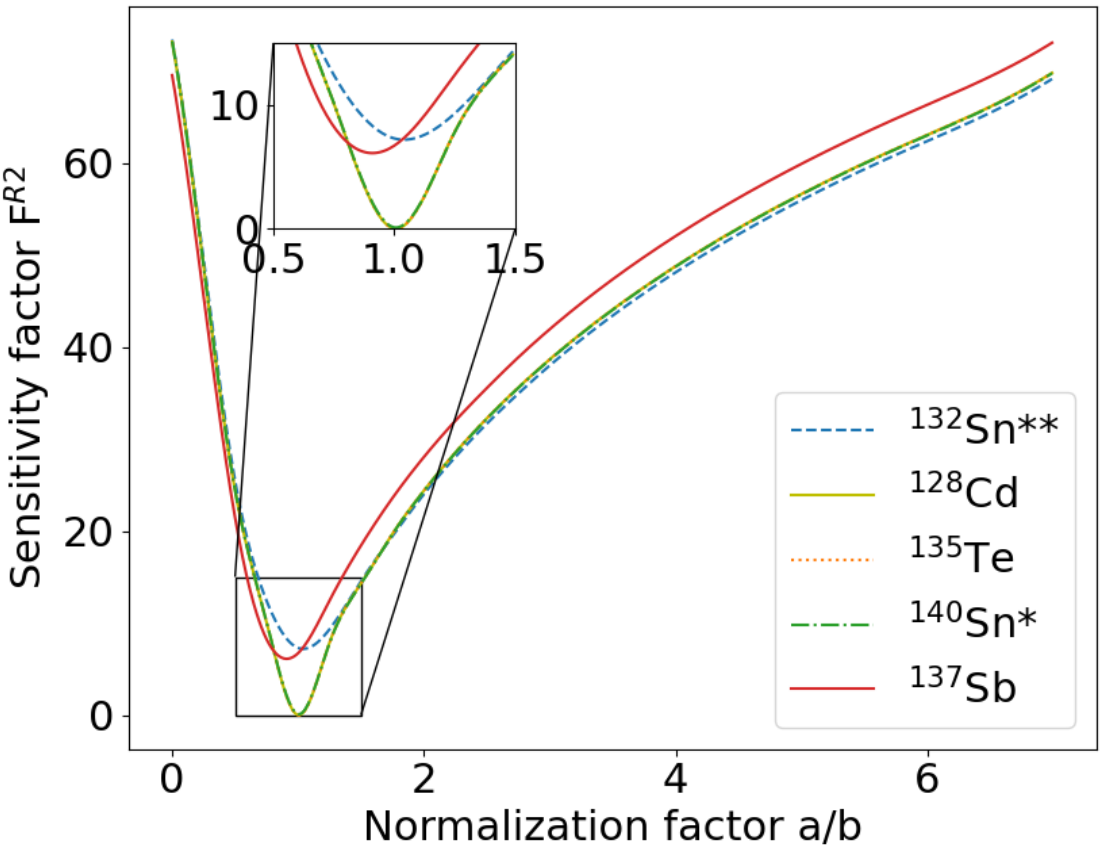

Figure 5.4: Comparison of sensitivity factors (using metric R2) as a function of normalization factor a/b for several different isotopes. The simulations were run in the custom r-process environment described in Section 5.4. The * indicates magic nuclei, and the ** indicates doubly-magic nuclei.

analysis is generally applicable to all *r*-process codes, networks, environments, etc.

5.6 Conclusion

The normalization of sensitivity study results is important to consider when comparing different studies. These results can be normalized such that F is minimized, which be a consistent standard with which we can compare studies. As well, applying normalization factors introduces an arbitrary scaling factor into the absolute sensitivity metrics (A1 and A2), which must then be dealt with, which we defined as calibration. This conclusion stems from the mathematical formulation we used, and as such the results are largely independent of the specific *r*-process code used. We therefore recommend that the relative metrics (R1 and R2) be used in future studies because in their case this scaling factor cancels out, making calibration unnecessary.

Metric	F_{default}	$F_{\text{minimized}}$	a/b	% difference
A1	44.7	38.3	0.75	14.3
A2	0.331	0.279	0.75	15.7
R1	17.5	17.5	0.95	0.01
R2	7.29	7.19	1.05	1.37

Table 5.1: Table of default (F_{default}, where $a/b = 1$) and minimized ($F_{\text{minimized}}$) sensitivity factors from Figure 5.2 (corresponding to ^{132}Sn), with their respective normalization factors a/b and the percent difference.

Isotope	F_{default}	$F_{\text{minimized}}$	a/b	% difference
^{132}Sn**	17.5	17.4	0.98	0.45
^{128}Cd	2.25×10^{-5}	2.25×10^{-5}	1.00	0.0
^{135}Te	0.004	0.004	1.00	0.0
^{140}Sn*	0.241	0.241	1.00	0.0
^{137}Sb	17.0	13.8	0.87	18.8

Table 5.2: Table of default (F_{default}, where $a/b = 1$) and minimized ($F_{\text{minimized}}$) sensitivity factors from Figure 5.3 (corresponding to metric R1), with their respective normalization factors a/b and the percent difference. The * indicates magic nuclei, and the ** indicates doubly-magic nuclei.

Isotope	F_{default}	$F_{\text{minimized}}$	a/b	% difference
^{132}Sn**	7.29	7.19	1.04	1.37
^{128}Cd	9.76×10^{-6}	9.76×10^{-6}	1.00	0.0
^{135}Te	0.002	0.002	1.00	0.0
^{140}Sn*	0.105	0.096	1.01	8.57
^{137}Sb	6.71	6.11	0.91	8.94

Table 5.3: Table of default (F_{default}, where $a/b = 1$) and minimized ($F_{\text{minimized}}$) sensitivity factors from Figure 5.4 (corresponding to metric R2), with their respective normalization factors a/b and the percent difference. The * indicates magic nuclei, and the ** indicates doubly-magic nuclei.

Chapter 6

SUMMARY, CONCLUSIONS AND FUTURE WORK

6.1 General Summary and Conclusions

Here I have undertaken an in-depth analysis into the presentation of *r*-process sensitivity studies. I have helped identify the potential for inconsistencies in how different studies report their results; the choice of sensitivity metric, as well as the way the results are scaled can have an effect. I therefore advocate for consistent reporting standards to ensure easy comparison.

Our recommendations include computing and presenting multiple sensitivity metrics, as there is no one metric that is the most useful in all situations (though I also identified an major advantage associated with the relative sensitivity metrics, these being R1 and R2).

With regards to normalization, we recommend that results be normalized so as to minimize the sensitivity factor, as this would avoid artificially inflating the sensitivity of any isotope studied. For those studies using absolute metrics (A1 and A2), the way these results are scaled must be made clear. To this end, reporting the maximum abundance in the resultant abundance patterns would be useful (this is referred to as calibration). It should be noted that metrics R1 and R2 do not require calibration (an arbitrary scaling factor is shown to cancel out in their mathematical formulations), and may be preferable to use for that reason.

6.2 Future work

In the process of benchmarking the SiRop code, I suggested that the problem of inconsistent reporting of sensitivity study results is larger than just the choice of metric or scaling of results. In particular, determining the initial conditions for a given study presented the greatest challenge. It would be prudent to try and establish consistent standards for initial conditions, which would help

not only with comparison of results, but the comparison of *r*-process codes. Such a project would benefit from a broader collaboration of groups researching the *r*-process.

The effects of normalization on the results of sensitivity studies hinted at some trends, especially how the closeness of the normalization factor that minimizes the sensitivity factor F to one is related to the sensitivity of the isotope, that could be studied in greater detail. A broader study of isotopes and how they are affected by normalization would be an interesting direction in which to take this research.

References

[1] A. Aprahamian, I. Bentley, M. Mumpower, and R. Surman, AIP Advances **4**, 041101 (2014).

[2] S. Brett, I. Bentley, N. Paul, R. Surman, and A. Aprahamian, Eur. Phys. J. **48**, 184 (2012).

[3] E. M. Burbidge, G. R. Burbidge, W. A. Fowler, and F. Hoyle, Rev. Mod. Phys. **29**, 547 (1957).

[4] A. G. W. Cameron, Astrophys. J. **62**, 9 (1957)

[5] A. G. W. Cameron, J. J. Cowan, and J. W. Truran, Astrophys. Space Sci. **91**, 235 (1983).

[6] S. E. de Mink and K. Belczynski, Astrophys. J. **814**, 58 (2015).

[7] K. Farouqi, K.-L. Kratz, B. Pfeiffer, T. Rauscher, F.-K. Thielemann, and J. W. Truran, Astrophys. J. **712**, 1359 (2010).

[8] S. Goriely, A. Bauswein, and H.-Th. Janka, Astrophys. J. Lett. **738**, L32 (2011).

[9] N. Itoh, Prog. Theor. Phys. **44**, 291 (1970).

[10] P. Jaikumar, B. S. Meyer, K. Otsuki, and R. Ouyed, A&A **471**, 227A (2007).

[11] M. Kostka, Ph.D. thesis, University of Calgary (2014).

[12] M. Kostka, N. Koning, Z. Shand, R. Ouyed, and P. Jaikumar, A&A **568**, A97 (2014).

[13] R. Mayle, J. R. Wilson, and D. N. Schramm, Astrophys. J. **318**, 288 (1987).

[14] J. D. McDonnell, N. Schunck, D. Higdon, J. Sarich, S. M. Wild, and W. Nazarewicz, Phys. Rev. Lett. **114**, 122501 (2015).

[15] B. S. Meyer, Annu. Rev. Astron. Astrophys. **32**, 153 (1994).

[16] B. S. Meyer, Phys. Rev. Lett. **89**, 231101 (2002).

[17] B. S. Meyer and J. S. Brown, Astrophys. J. **112**, 199 (1997).

[18] P. Möller, W. D. Myers, W. J. Swiatecki, and J. Treiner, At. Data Nucl. Data Tables **39**, 225 (1988)

[19] M. R. Mumpower, G. C. McLaughlin, and R. Surman, Phys. Rev. C **86**, 035803 (2012).

[20] M. R. Mumpower, R. Surman, D.-L. Fang, M. Beard, P. Möller, T. Kawano, and A. Aprahamian, Phys. Rev. C **92**, 035807 (2015).

[21] M. R. Mumpower, R. Surman, G. C. McLaughlin, and A. Aprahamian, Prog. Part. Nucl. Phys. **86**, 86 (2016).

[22] R. Ouyed, J. Dey, and M. Dey, A&A **390**, L39 (2002).

[23] I. V. Panov and H.-Th. Janka, A&A **494**, 829 (2009).

[24] Y.-Z. Qian and G. J. Wasserburg, Astrophys. J. **588**, 1099 (2003).

[25] M. Samyn, S. Goriely, P.-H. Heenen, J. M. Pearson, and F. Tondeur, Nucl. Phys. A **700**, 142 (2002).

[26] Z. Shand, M.Sc. thesis, University of Calgary (2016).

[27] Z. Shand, R. Ouyed, N. Koning, C.-J. U. Osakwe, I. Dillmann, R. Krücken, and P. Jaikumar, Phys. Rev. C (Manuscript submitted for publication) (2020).

[28] C. Sneden, J. J. Cowan, and R. Gallino, Annu. Rev. Astron. Astrophys. **46**, 241 (2008).

[29] A. Sobiczewski and Y. A. Litvinov, Phys. Rev. C **90**, 017302 (2014).

[30] R. Surman, J. Beun, G. C. McLaughlin, and W. R. Hix, Phys. Rev. C **79**, 045809 (2009).

[31] R. Surman, M. R. Mumpower, J. Cass, I. Bentley, A. Aprahamian, and G. C. McLaughlin, Eur. Phys. J. WOC **66**, 07024 (2014).

[32] E. Witten, Phys. Rev. D **30**, 272 (1984).